Top Curr Chem (2014) 339: 1–54
DOI: 10.1007/128_2012_393

Published online: 18 December 2012

Emerging Areas in Atmospheric Photochemistry

Christian George, Barbara D'Anna, Hartmut Herrmann, Christian Weller, Veronica Vaida, D.J. Donaldson, Thorsten Bartels-Rausch, and Markus Ammann

Abstract Sunlight is a major driving force of atmospheric processes. A detailed knowledge of atmospheric photochemistry is therefore required in order to understand atmospheric chemistry and climate. Considerable progress has been made in this field in recent decades. This contribution will highlight a set of new and emerging ideas (and will therefore not provide a complete review of the field) mainly dealing with long wavelength photochemistry both in the gas phase and on a wide range of environmental surfaces. Besides this, some interesting bulk photochemistry processes are discussed. Altogether these processes have the potential to introduce new chemical pathways into tropospheric chemistry and may impact atmospheric radical formation.

Keywords Cloud chemistry · Dust · Heterogeneous chemistry · Ice photochemistry · Organic aerosols · Urban grime · Vibrational overtone absorption

C. George (✉) and B. D'Anna
Université de Lyon, Lyon 69626, France

CNRS, UMR5256, IRCELYON, Institut de recherches sur la catalyse et l'environnement de Lyon, Villeurbanne 69626, France
e-mail: christian.george@ircelyon.univ-lyon1.fr

H. Herrmann and C. Weller
Leibniz-Institut für Troposphärenforschung (IfT), Chemistry Department, Permoserstr. 15, 04318 Leipzig, Germany

V. Vaida
Department of Chemistry and Biochemistry and CIRES, University of Colorado, Boulder, CO 80309, USA

D.J. Donaldson
Department of Chemistry, University of Toronto, 80 St. George Street, Toronto, ON, Canada M5S 3H6

T. Bartels-Rausch and M. Ammann
Laboratory of Radiochemistry and Environmental Chemistry, Paul Scherrer Institute, Villigen, Switzerland

Contents

1 Introduction

From a chemical perspective, the atmosphere may be described as a giant, fairly well-mixed photochemical reactor, in which most of the processes are initiated by sunlight. As the light source in this context, the sun may be considered as a spherical blackbody emitter at $T \sim 5{,}770$ K outside the atmosphere. One of the most important photochemical processes in the atmosphere is the generation of free radicals (such as the hydroxyl radical, OH) through the UV photolysis of precursors such as ozone or carbonyl compounds. These reactions have been the focus of numerous studies and will not be covered here [1]. The present contribution will deal mainly with reactions which may occur at longer wavelengths than those initiated by direct photolysis, such as vibrational overtone initiated processes and photosensitized reactions. As illustrated in Fig. 1, visible light photons are significantly more abundant in the atmosphere than UV photons, since several atmospheric constituents (such as O_2 and O_3) absorb UV strongly, and thus filter out the short wavelength light emitted by the sun. Nevertheless, a few important UV-triggered processes, for example reactions of non-conventional precursors in aqueous systems, will also be discussed as the authors regard this as an emerging field in atmospheric photochemistry.

An atmospheric photochemical reaction starts with the absorption of a photon by an atmospheric molecule at an appropriate wavelength of available light, producing an excited electronic or vibrational state. Typically, absorption of a photon by a singlet ground state (S_0) will initially produce primarily a singlet excited state (S_1), because the transition from a singlet to a triplet state (i.e., a transition in which electron unpairing takes place with a changing spin) is spin-forbidden and may only take place with a very low probability [2]. However, a triplet state of lower energy

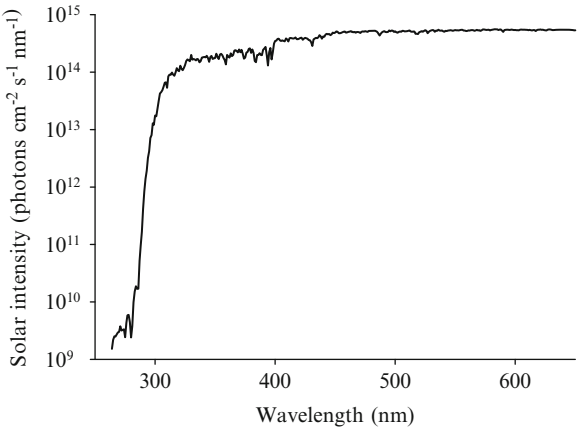

Fig. 1 Photon flux in the middle troposphere as a function of wavelength

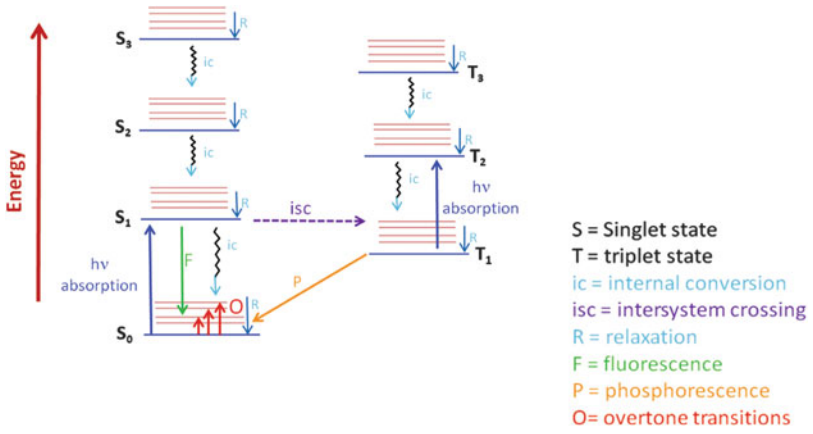

Fig. 2 Schematic Jablonski diagram

may be created by intersystem crossing (induced by spin-orbit coupling). In general, the energy absorbed during the electronic transition can be dissipated by a variety of photochemical and photophysical processes, such as fluorescence, collisional deactivation, collisional or collisionless transition to a lower electronic state, or chemical reaction (dissociation or rearrangement). Radiationless transitions may connect the excited electronic state prepared by photon absorption with the ground state as shown in Fig. 2. In such instances, the system is prepared in its ground electronic state with large excess of thermal energy or in another configuration favorable to photochemical product formation. In contrast, vibrational overtone excitation initiated by red light prepares the system "cold," in its ground electronic state, with sufficient vibrational energy for reaction but little or no excess vibrational or thermal excitation. Several of these energy transfer pathways are illustrated in the Jablonski diagram in Fig. 2.

Photodissociation leads to bond breaking and is of central importance in atmospheric chemistry for free radical production. Photodissociation is well studied for electronic transitions, and this will not be reviewed here. Direct excitation of vibrationally excited states, which have sufficient energy to dissociate, can occur with visible solar radiation; this process is discussed below.

Energy transfer between two molecules is also an important deactivation pathway for excited states, allowing photosensitized reactions to take place. Such a process can be simply described as

$$\mathrm{D} + h\nu \rightarrow \mathrm{D}^* \tag{1}$$

$$\mathrm{D}^* + \mathrm{A} \rightarrow \mathrm{D} + \mathrm{A}^* \tag{2}$$

where the excited molecule D* transfers its energy to A, producing the excited state A*. The sequence of (1) and (2) is described as photosensitization of A by the photosensitizer D. In another way of looking at this, D* has been quenched by A. Energy transfers are named as a function of the spin multiplicity of the excited states of D* and A*:

$$\text{singlet-singlet energy transfer: } {}^1\mathrm{D}^* + {}^1\mathrm{A} \rightarrow {}^1\mathrm{D} + {}^1\mathrm{A}^* \tag{3}$$

$$\text{triplet-triplet energy transfer: } {}^3\mathrm{D}^* + {}^1\mathrm{A} \rightarrow {}^1\mathrm{D} + {}^3\mathrm{A}^* \tag{4}$$

Such processes have been the focus of many studies, especially in liquid phases. The triplet–triplet process is interesting as it allows excitation of the triplet state of the molecule A that would otherwise be inaccessible (for instance due to a poor intersystem crossing $S_1 \rightarrow T_1$). This then may increase the yield of a reaction but also initiate specific reactions. If the energy required to excite the initial state ^{1}D* (prior to its transition to the triplet state) is lower than the excitation energy of ^{1}A*, then photosensitized reactions of ^{3}A* become possible at longer wavelengths [3].

Let us illustrate this chemistry with an example. Benzophenone is a well-known photosensitizer, which will phosphoresce at low temperature (77 K) after excitation in the range 360–370 nm. This phosphorescence of benzophenone is quenched by adding a polyaromatic hydrocarbon (PAH) such as naphthalene; phosphorescence is then observed from this species even though it has no absorption band around 360–370 nm. Such observations clearly describe the activation at wavelengths otherwise transparent for a given medium. This sequence of processes can be described as follows:

$(C_6H_5)_2CO + h\nu \rightarrow {}^1(C_6H_5)_2CO^*$	Light absorption by the photosensitizer
${}^1(C_6H_5)_2CO^* \rightarrow {}^3(C_6H_5)_2CO^*$	Intersystem crossing producing the triplet state
${}^3(C_6H_5)_2CO^* + {}^3PAH \rightarrow {}^1(C_6H_5)_2CO + {}^3PAH^*$	Triplet–triplet energy transfer to the added PAH
${}^3PAH^* \rightarrow {}^1PAH + h\nu$	Deactivation of the triplet state – here by a photophysical process such as phosphorescence

In this example, the triplet state of benzophenone is quenched by the added PAH. However oxygen is also known to be an effective triplet state quencher:

$$D^*(T_1) + {}^3O_2 \rightarrow D(S_0) + {}^1O_2 \quad (5)$$

where, despite quenching of D*(T_1), reactive singlet oxygen is produced by energy transfer to the ground state triplet state of oxygen.

Light absorption by a molecule (R) promotes an electron to a higher energy level, and this may affect the redox properties of this molecule. For example, this molecule may become a better electron donor (reducing agent) in its excited state as compared to its ground sate. In contrast, the electron vacancy created by the electronic transition might exhibit better electron acceptor properties and thereby be a better oxidizing agent. These two features, known as photoinduced electron transfer, can be described in the case of R reacting with the molecule M as follows:

$R + h\nu \rightarrow R^*$	Light absorption by R
$R^* + M \rightarrow R^{\bullet+} + M^{\bullet-}$	R acts as electron donor and is oxidized
$R^* + M \rightarrow R^{\bullet-} + M^{\bullet+}$	R acts as electron acceptor and is reduced

As mentioned above, photoinduced electron transfer occurs via electron exchange interactions, which require overlap of the electronic densities of both molecules R and M, and is therefore a process occurring over short distances.

While the above examples are often used to describe homogeneous organic photochemistry, there are processes that are specific to heterogeneous processes involving solid oxides (such as those found in mineral dust), i.e., heterogeneous photocatalysis [4, 5]. Heterogeneous photocatalysis has been reported in gas and liquid phases (aqueous and organic). Classically, the overall process can be broken down into five independent steps:

1. Transfer of the reactants in gas or liquid phase to the surface
2. Adsorption of at least one of the reactants
3. Reaction in the adsorbed phase
4. Desorption of the product(s)
5. Removal of the products from the interface region

While these steps are common to all heterogeneous processes (such as the uptake of a gas by a liquid droplet or heterogeneous catalysis), step 3 is where the photocatalytic nature of certain metal oxides plays a role. In fact, when a semiconductor catalyst (SC), such as a metal oxide (TiO_2, ZnO, ZrO_2, CeO_2,. . .) or sulfide (CdS, ZnS,. . .), is illuminated with photons carrying energy equal or in excess of its band gap, absorption of light promotes one electron into the conduction band, creating an electron–hole pair (Fig. 3) similar to photoinduced electron transfer. The oxide may transfer its electron to any adsorbed electron acceptor (thereby promoting its reduction), while the hole (or the electron vacancy) may accept an electron from an adsorbed donor (promoting its oxidation).

In the case of an oxide exposed to ambient air, adsorbed oxygen (O_2) will act as the dominant electron acceptor and produce the highly reactive superoxide radical anion (O_2^-). Simultaneously, adsorbed water will be oxidized to hydroxyl radicals

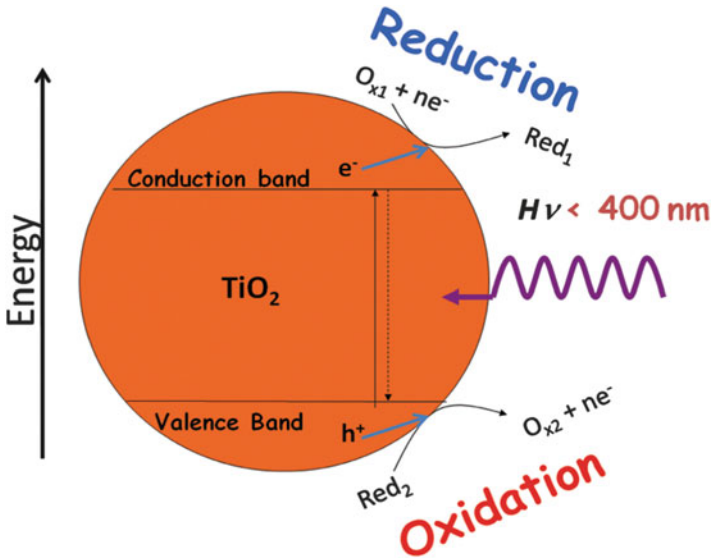

Fig. 3 Schematic of a photocatalytic process. When illuminated with light of energy higher than the band gap, electron–hole pairs are created in a semiconductor, thus allowing chemical reactions on its surface

(OH). Hence the surface of such an illuminated oxide will be highly reactive toward a series of organic (and adsorbed) compounds such as volatile organic compounds (VOCs) often encountered in atmospheric chemistry.

Both photosensitized reactions and heterogeneous photocatalysis have been the focus of many studies and reviews for the degradation of organic and inorganic species in natural terrestrial surface water. This review will discuss their potential importance in the atmosphere for two distinct cases – photochemistry of mineral dust (which contains oxides able to initiate photocatalysis) and organic or carbonaceous aerosols (which contain aromatic compounds or humic like substances able to act as photosensitizers). Additionally, direct photochemistry of unconventional precursors, i.e., iron-dicarboxylic acid anionic complexes, will also be dealt with.

2 Vibrationally Excited Photochemical Processes in the Gas Phase

Like all photolysis reactions, those initiated by vibrational overtone absorption are analyzed as first-order kinetic processes with a photochemical rate, J, which depends upon the absorption coefficient $\sigma(\lambda)$ of the absorbing compound, the

quantum yield (that is, the ratio of dissociation events to the number of photons absorbed for the dissociation $\varphi(\lambda)$), and the available photon flux $I(\lambda)$:

$$J = \int_{\lambda} \sigma(\lambda)\varphi(\lambda)I(\lambda)\mathrm{d}\lambda \tag{6}$$

In the Earth's atmosphere, visible light ($\lambda > 400$ nm) is present to some extent at all altitudes and solar zenith angles. Although such radiation may be sufficiently energetic to rupture weaker chemical bonds, it is generally not in the correct wavelength range to induce electronic transitions of the chemical compounds present in the atmosphere. However, in polyatomic molecules containing O–H, C–H, and N–H groups, the small mass of the hydrogen atom means that X–H stretching frequencies are considerably higher than those of other vibrational modes. In the absorption spectrum this feature and the generally large anharmonicities associated with such X–H stretches give rise to the appearance of overtone transitions with appreciable intensity [6]. Of particular atmospheric importance are the OH stretching overtones of alcohols, organic acids, and peroxy-compounds which, for the most part, are transparent to the ultraviolet wavelengths present in the lower atmosphere. Such species are emitted directly into the troposphere, but are also products of atmospheric oxidation reactions initiated by the OH radical.

The OH stretching frequency lies in the range 3,600–3,000 cm^{-1} and the anharmonicity is approximately 85 cm^{-1} [7–10]. The light hydrogen oscillator and the large anharmonicity value give rise to higher overtone transitions (generally by the $v = 3$ level) becoming sufficiently separated from the rest of the molecular vibrations to be treated by the "local mode" approximation [11], in which each X–H vibration is taken to be an independent anharmonic oscillator. Spectroscopically, the latter condition means that overtone absorptions are well separated from other absorptions, as shown for the case of nitric acid in Fig. 4.

The energies accessed by OH vibrational overtone transitions above $v_{\mathrm{OH}} = 3$ or so are sufficient to initiate reactions. However, the challenge of initiating reaction by vibrational overtone excitation lies in the low cross section of vibrational overtone transitions, which are typically three to six orders of magnitude lower in intensity at chemically relevant regions compared to electronic transitions in the ultraviolet. Intensities of vibrational overtone transitions generally decrease by an order of magnitude with each quantum of excitation [12]. Nevertheless, under conditions in which ultraviolet photochemistry is limited due to the lack of appropriate light and/or molecular absorptions, such overtone-initiated chemistry may play an important role in the atmosphere [13–16]. As mentioned above, alcohols, organic acids, and peroxy-compounds all possess OH stretching overtone transitions in the visible spectral region.

What distinguishes vibrational overtone initiated chemistry from that driven by electronic excitation is that the chemistry takes place exclusively in the ground electronic state. In general, following absorption of a photon, chemistry is in competition with energy dissipation; in the lower atmosphere this is often driven

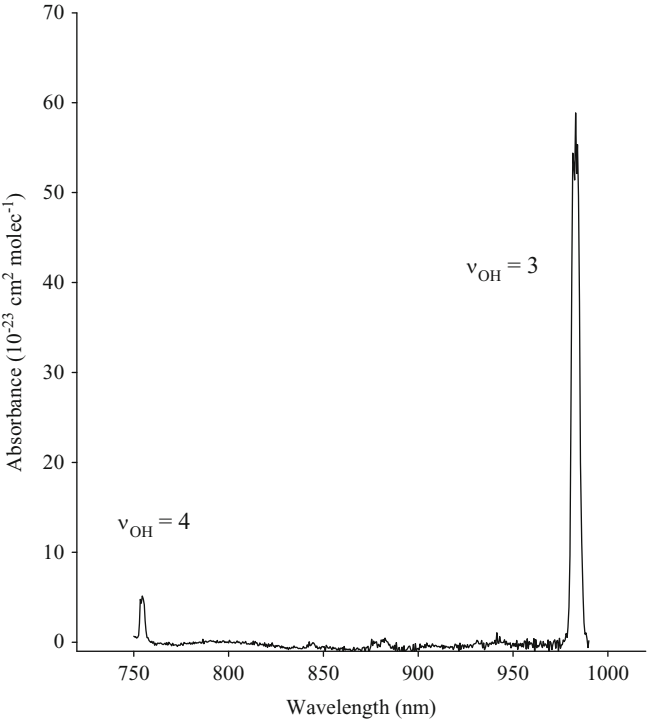

Fig. 4 Absorption spectrum of gas phase nitric acid in the near IR region, showing the overtone transitions to the $v = 3$ and $v = 4$ levels of the OH stretch. Adapted from Fig. 1 of [7]

by collisional energy loss. Electronic transitions of atmospherically important molecules such as NO_2 and O_3 access dissociative states with very short lifetimes compared to the collisional time. By contrast, overtone chemistry requires energy flow away from the initially excited mode (i.e., the OH stretch vibration) into adjacent regions of the molecule. This intramolecular vibrational redistribution (IVR) process takes place on the time scale of many vibrational periods, setting a limit for the effectiveness of chemistry, depending on local temperature and pressure. The efficiency of such processes is higher at high altitude where low pressure limits the efficiency of collisional deactivation.

2.1 Bond Cleavage Reactions

This type of process has been studied reasonably extensively for systems in which an OH moiety is adjacent to a weak bond, such as O–O or O–N. Vibrational overtone transitions to states with 3–6 quanta of OH stretch occur in the near-infrared to visible region of the spectrum and deliver sufficient energy to break the

adjacent weak bond in several atmospherically important molecules, such as the O–O bond in peroxy-compounds such as HOOH [17–20] or the N–O bond in HNO_x type compounds (HONO, $HONO_2$, HO_2NO_2) [19, 21–24]. These compounds are very important sequestering agents for NO_2 (which forms ozone through photolysis to NO + O and recombination of the O-atom with O_2) and OH (the primary agent for oxidation reactions in the troposphere). Therefore, understanding their formation and destruction reactions is critical to being able to predict air quality and the oxidative ability of the lower atmosphere.

In nitric acid ($HONO_2$), for example, initial excitation of an OH stretching motion at $v_{OH} \geq 5$ accesses energies above the dissociation limit to OH + NO_2 [19]. In the absence of collisional de-excitation, this energy will "flow" from the initially excited vibration throughout the molecule, via IVR. During this equilibration process, sufficient energy may be deposited in motion along the N–O dissociation co-ordinate to induce bond cleavage. An upper limit to the enhancement due to vibrational overtone pumping of the photolysis rate of HNO_3 has been calculated based on vibrational overtone cross sections [19, 21–24] with an assumed quantum yield of 1. At 20 km altitude and at about 92° zenith angle the calculated enhancement for the photolysis rate of HNO_3 is about 30%.

In the well-studied case of hydrogen peroxide, H_2O_2, overtone levels of the OH stretch may be excited at energies exceeding the O–O bond dissociation energy of about 215 kJ mol^{-1}. Reaction occurs by energy flow from the initially excited OH stretch local mode to the weak O–O bond to give the OH radical. Simulations of the dynamics following overtone excitation have shown that the initial step in the dissociation is a rapid coupling of the OH stretching and OOH bending modes. This type of coupling seems to allow flow of energy out of the OH moiety and into the weak bond. Similar reaction mechanisms were used to explain dissociation following vibrational overtone pumping in other, similar compounds.

In the case of HO_2NO_2 (peroxynitric acid or PNA) the thermochemical dissociation limit is reached at energies somewhat below the $v = 3$ level of the OH stretch. Thermally-assisted dissociation becomes possible from the $v = 2$ level as well, depending upon the temperature. This process has been shown to occur in laboratory measurements, using action spectra of HO_2 formation as a function of the excitation wavelength of PNA [23, 25]. These measurements show temperature-dependent formation of HO_2 from the $v = 2$ level of OH stretch, and a smaller but temperature-invariant formation efficiency from the $v = 3$ level. Inclusion of overtone-initiated dissociation of PNA from OH stretching vibrational levels $v \geq 2$ in atmospheric models has shown this process to be an important source for HO_x in the free troposphere and lower stratosphere [26–30]. Reaction with HO_x radicals is a dominant sink in photochemical loss cycles of ozone in the lower stratosphere. The vibrational overtone process is calculated to produce a 20–60% increase in HO_x at high latitudes in the spring, leading to a greater sensitivity of ozone to atmospheric perturbations such as increased water vapor.

The postulated mechanism for energy flow from the OH to the weak bond by IVR in examples where a weak bond ruptures following overtone excitation appears to be more complicated in HONO and $HONO_2$. Gerber and co-workers [22] have

carried out dynamical simulations of the molecular motion following overtone excitation and find that IVR to the N–O bond is not the only important process taking place. Intramolecular hopping of the hydrogen atom from one oxygen atom to another also occurs on very fast time scales. Interestingly, this H atom hopping occurs at energies well below the bond dissociation energy for the O–H bond, so the process is a concerted reaction where one O–H bond breaks while another is being generated.

2.2 *Rearrangement Followed by Dissociation*

In addition to direct bond cleavage, molecules with a high degree of internal excitation may undergo rearrangements followed by dissociation to molecular products. This is the idea behind the well-known phenomenon of thermal (unimolecular) decomposition. It is similar in initiation to the bond cleavage process described above, with the important distinction that such "concerted" chemistry may occur at energies lower than an individual bond dissociation energy. For example, malonic acid undergoes thermally-induced decarboxylation at relatively low temperatures [31]; this chemistry may also be induced by OH stretching overtone excitation [32]. Similarly, sulfuric acid has been predicted to undergo a unimolecular dehydration reaction to form SO_3 and H_2O following excitation to $v \geq 4$ of an OH stretching vibration [33]. This level corresponds to energies well below the weakest individual bond in the acid. The decomposition of H_2SO_4 is also known to occur thermally but at very high temperatures [34].

Sulfuric acid is one of the main constituents of atmospheric aerosols, of enormous interest because of the large and as yet not completely understood effect these aerosols have on the planet's climate. Sulfate aerosols form at low altitude in the troposphere and the cool stratosphere and evaporate as they ascend towards the warm stratopause. Modeling studies led to the conclusion that sunlight-initiated chemistry of H_2SO_4 must occur at high altitude to explain measured stratospheric SO_2 concentrations [35]. Although the lowest electronic transitions are not accessible to the available solar radiation [36], several OH vibrational overtone transitions do absorb in the actinic region and are therefore available to activate this molecule [33, 37]. Below 70 km the relevant photodissociation mechanism for H_2SO_4 is initiated by absorption of red light by OH vibrational overtones, specifically by $v_{OH} = 4$ and 5 [38–40].

The possibility of vibrational overtone initiated dehydration of sulfuric acid to $SO_3 + H_2O$ has been investigated by spectroscopic [37, 41, 42] and theoretical [38, 43, 44] methods. Dynamical simulations of the dehydration reaction find two mechanisms to be operative in this reaction: a fast loss of H_2O initiated by hydrogen atom hopping, similar to that found following nitric acid excitation, and a slower dissociation, occurring after full or partial IVR [43, 45]. Based on these mechanisms and rates, the dehydration of sulfuric acid is very effective under conditions of the upper stratosphere and mesosphere [46]. The rate of dehydration thus obtained is

sufficient to explain atmospheric observations of the SO_2 vertical profile and the formation of large concentrations of cloud condensation nuclei at the top of the aerosol layer in polar spring or in mid-latitude air of recent polar origin [39, 40]. In this example, no alternative photochemical process is available in the stratosphere, since the electronically excited states of H_2SO_4 are at very high energy [33, 37]. Sunlight-initiated reactions of sulfuric acid will be important beyond the Earth's atmosphere, notably on Venus where sulfuric acid clouds are known to exist [47].

Concerted photoreactions initiated by OH vibrational overtone excitation have also been proposed to occur in organic acids and their reaction mechanisms and rates have recently been investigated by theoretical and spectroscopic methods [10, 42, 48]. The early time dynamics of vibrationally excited pyruvic and glyoxylic acids have been studied by a combination of "on-the-fly" dynamics simulations and cavity ringdown spectroscopy [48–50]. These combined studies concluded that decarboxylation of the ketoacids occurs on sub-picosecond time scales following OH overtone excitation. A strong correlation between structure and reactivity was observed: conformers that possess intramolecular hydrogen bonded structures react on excitation of the third and fourth OH overtone by hydrogen atom chattering, while nearly isoenergetic conformers of *trans* geometry do not react by a fast process. The "chattering" mechanism involves rapid hydrogen atom exchanges between donor and acceptor oxygen atoms. In contrast with hydrogen atom "tunneling," chattering is a classically allowed process occurring above any exchange barrier. Chattering proceeds on a time scale set by the vibrational frequency and is consequently much faster than the tunneling motion [51].

The examples discussed above illustrate the utility of vibrational overtone excitation by red sunlight in atmospheric photochemistry. The low absorption cross-section of vibrational overtones limits the importance of such light-initiated chemistry. However, when reactive electronic states are high in energy (as is the case with most alcohols and acids) or when UV radiation is suppressed at high solar zenith angles, vibrational overtone initiated photochemistry has been used to explain discrepancies between measurements and model results.

3 Aerosol Photochemistry

3.1 Organic Aerosols

Organic material comprises a large fraction of the sub-micron aerosol mass ranging from 20% to 50% in continental mid-latitudes and up to 90% in tropical forested areas [52–54]. Significant amounts of carbonaceous aerosols are also observed in the upper troposphere [55]. Organic particles may have a direct radiative forcing through scattering and absorption of solar and infrared radiation and an indirect radiative forcing by affecting cloud formation and by inducing changes in cloud properties [56]. Organic aerosols are also related to health effects due partly to the

presence of toxic compounds, such as polycyclic aromatic hydrocarbons (PAHs), which are known for their carcinogenic and mutagenic potency to humans and animals [57–59].

Chemical reactions proceeding at the surface or within the bulk of aerosol particles can influence atmospheric gas phase chemistry as well as the properties of the particles themselves, including their effects on climate and human health. So far, the atmospheric chemistry community has mostly considered heterogeneous or multiphase reactions under dark conditions between reactive atmospheric gas phase oxidants and organic compounds known to be present in the particulate phase. Many laboratory studies have used oxidation of PAHs and/or soot [60–87], oleic acid, and other organic compounds as proxy systems to understand mechanisms and kinetics of these reactions and to assess their significance [88–90].

This focus on dark reactions has ignored the fact that organic sub-micron aerosols absorbing near-UV and visible light are ubiquitous in the atmosphere, including soot as the most extreme example. Enhanced UV absorption features were observed, for instance, in remote areas as well as in polluted environments [41, 91–95]. Reference [91] showed strong spectral dependence of the light absorption by organic aerosols in the UV. Similar absorption attributed to organics has been reported in several other measurements (e.g., [41, 94–102]). Sources of this absorbing material in organic aerosols may include the resuspension of soil-derived material by wind erosion or combustion processes such as biomass burning or fossil fuel combustion [91, 103–107]. Laboratory studies have noted the formation of solar light absorbing material following a few hours of oxidation in the condensed phase. These studies have mostly concentrated on bulk solutions, with only a few observing reaction in the aerosol phase directly (e.g., [92, 108–114]). During processing, initially non-absorbing organic compounds are converted into compounds that display significant absorption in the UV and even visible regions. The presence of such light absorbing material in particles may enable photo-induced and/or photo-sensitized processes. While a significant body of literature exists on photo-induced charge and/or energy transfer in organic molecules of relevance in terrestrial water chemistry, biochemistry, and water waste treatment [115–117], relatively little work exists in the field of atmospheric aerosols, where only a few groups have investigated the chemistry of the light-absorbing organic material present in aerosols [118–123].

Stemmler et al. [124] used humic acid aerosols as a proxy for HULIS (HUmic-LIke Substances) to study the photo-induced conversion of NO_2 into HONO, which was previously observed on various organic condensed films [125–128]. The light-induced process was able to release more HONO than was obtained under dark conditions, similar to what was observed for other organic substrates. The amount of the enhancement is not dramatic: even if the whole organic aerosol was composed of humic acids, for typical aerosol surface concentrations of 100 $\mu m^2\ cm^{-3}$ for rural and 1,000 $\mu m^2\ cm^{-3}$ for urban conditions, only1.2 and 17 pptv h^{-1} of HONO would be formed on aerosol surfaces in rural and urban environments, respectively. These values represent upper limits as in reality rural and urban continental aerosol is composed only of 20–50 mass % of organic matter. On the

other hand, HONO production reported for daytime at ground and over forested or rural sites is up to 170–500 ppt h^{-1} [127] or in urban environments up to 2 ppb h^{-1}. Stemmler et al. [124] suggested that photochemical HONO formation on organic aerosol is unlikely to be an important contributor to the HONO formation observed in the boundary layer. In exceptionally highly polluted areas, such as in biomass burning plumes or in mega-cities, environmentally relevant HONO photo formation rates on organic aerosol may occur.

Similar light-induced production of HONO upon exposure to NO_2 has been observed on soot [129]. The source strengths estimated for atmospheric conditions are comparable to those for humic acids. The process therefore represents only a small source of HONO in the gas phase. However, Monge et al. demonstrated that HONO production on soot does not cease quickly due to deactivation of reactive species under irradiation as it does under dark conditions, and so soot may act as a photoactive substrate over its entire life cycle in the atmosphere.

The need for investigating the role of organic aerosols as a possible sink for ozone has been suggested in the past by Jacob et al. [130], since this type of particle has a sufficient source strength and potentially a high enough reactivity to provide a significant sink for ozone in the continental boundary layer. The photo-reactivity of ozone with humic acid aerosol was investigated by D'Anna and co-authors [131]. The authors concluded that the light-induced process is not able to affect gas phase concentrations of ozone in the troposphere. Nevertheless, the amount of ozone reacted may be significant for aerosol aging [131] because OH radical is produced upon electron transfer from the organic substrate to ozone [132].

Because significant differences exist between terrestrial aquatic humic acids (such as those used in most laboratory experiments on HULIS) and aerosol humic-like substances (lower aromaticity, lower molecular weight, and better droplet activation ability) [133], the photo-induced reactivity of genuine atmospheric HULIS extracts with gas phase ozone was investigated by the same group (Fig. 5) [134]. The authors used HULIS collected from winter filters in Chamonix, which are strongly influenced by local emission of residential wood burning. The experimental results indicate a much higher photo-induced uptake of ozone on films prepared with such HULIS extracts than with films of humic acids. TOC (Total Organic Carbon) analysis of the extract before and after photo-treatment showed a reduction of the total amount of carbon; emission of VOCs and CO was interpreted to be a consequence of ozonation [135], photolysis [136–138], and a combination of both processes [131]. Functional group analysis suggested the formation of carbonyl and carboxylic groups under the combined action of light and ozone [134].

As in the case of NO_2, soot particles also exhibit photoenhanced O_3 uptake, in both the UVA and the visible wavelength ranges [139]. While under dark conditions over long times O_3 shows only very low reactivity, the study by Zelenay et al. [139] demonstrates that rates of O_3 uptake are orders of magnitude higher under light than under dark conditions. Surprisingly, this enhanced oxidation was accompanied by an increase in the contact angle of water, i.e., the surface became less hydrophilic. X-Ray absorption spectroscopy revealed a reduction in oxygenated organic components upon irradiation, suggestive of decarboxylation processes and

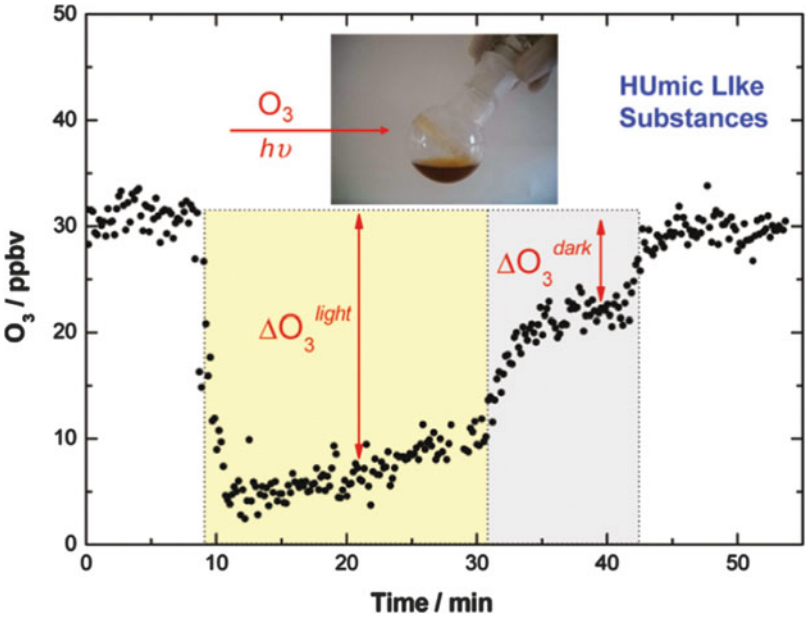

Fig. 5 Evolution of the O_3 gas phase mixing ratio (*black dots*) as a function of time after contact with a film made of HULIS extracted from organic aerosols collected in the winter season at Chamonix, France (*photo*). An ozone reduction of approximately 25 ppbv is observed during UVA irradiation

evaporation of highly oxidized small OVOC and CO_2. This demonstrates that indirect photochemistry affects the subtle feedbacks among oxidation, photochemistry, and hydroscopic properties (and thus climatic effects) of particles.

While the experiments related to photosensitized processes reviewed above were concerned with inorganic oxidants from the gas phase, the question arises as to whether comparable processes would occur with organic acceptors. Rouviere et al. [140] noted significant light induced degradation of succinic acid in deliquesced ammonium sulfate particles in the presence of small amounts of benzophenone. This effect was also confirmed by experiments in aqueous solution showing efficient triplet quenching by succinic acid. This has led to the idea that photosensitized processes may play a role in secondary organic aerosol (SOA) formation. Recently, Monge and co-authors [141] proposed that heterogeneous reactions activated by light lead to fast uptake of non-condensable VOCs at the surface of particles when traces of a photosensitizer were in the aerosol seeds. Seed particles containing succinic acid and only traces of humic acids showed a rapid diameter growth when irradiated with near-UV light in the presence of a terpene. An enhanced effect was reported when traces of nitrate were added to the seed particles, while no growth was observed, under the same experimental conditions, if the seed particles contained only carboxylic acids. Replacing air by pure N_2 (containing traces of O_2 up to 50 ppmv) drastically reduced the photo-induced particle growth,

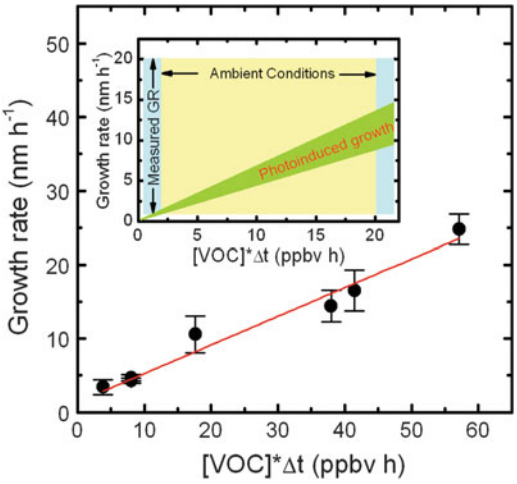

Fig. 6 Experimental results from an aerosol flow tube experiment using humic acid/succinic acid/NH_4NO_3 (1:10:1 by weight) as seed particles exposed to 320 ppbv of limonene and to UV-A light. The residence time of the aerosol in the flowtube is 9.7 min. Calculated growth rate values as a function of the product between limonene concentration and residence time in the flow tube. These values are calculated by considering the photoenhanced growth ($GR = \Delta D_m/\Delta t$) vs VOCs concentration per exposure time. Values are evaluated for solar irradiance. The *inset* shows growth rate (GR) values given by the photoinduced process compared to the literature GRs values (1–20 nm h^{-1}). Ambient conditions are assumed to vary from 0.2 ppbv to 2 ppbv of limonene and exposure to solar irradiance for 10 h, in the 300–420 nm (near-UV) wavelength range

suggesting that O_2 is involved in the reaction mechanism, a role well known from previous studies on DOM- and humic-containing waters [142–144]. Figure 6 shows how the particle growth rate depends upon the product between limonene concentration and residence time in the aerosol flow tube for typical solar irradiance. Ambient conditions are assumed to vary from 0.2 to 2 ppbv of limonene; the exposure to solar irradiance is approximated to 10 h per day in the 300–420 nm (near-UV) wavelength range. Therefore the experimentally determined growth rate values matched field observations, suggesting that this photochemical process can provide a new and unaccounted pathway for atmospheric particle growth and should be considered by models [141]. These laboratory results represent a radical change from the traditional view of gas phase oxidation of VOCs by atmospheric oxidants leading to SOA formation.

3.2 Mineral Dust

Estimates of emissions of mineral dust into the atmosphere presently lie around 1,500–2,000 Tg per annum [145] making mineral dust an important component of the coarse fraction of atmospheric aerosol and explaining its significant impact on

several atmospheric processes including radiative forcing and the modification of photochemical cycles. The direct radiative forcing effect (due to scattering and absorption of incoming solar radiation) is accompanied by an indirect effect as clay and silica particles are effective condensation and ice nuclei [146, 147], which can ultimately affect cloud structure and precipitation patterns [148]. The indirect effect will be modified by the physical state of the mineral dust particles, which will be influenced by chemical ageing during atmospheric transport.

Uptake of several trace gases (such as N_2O_5, NO_x, HNO_3, SO_x, O_3) on mineral dust particles and their surrogates has recently received attention [149–155]. Of particular importance is the conversion of SO_2 into sulfates and of NO_x and NO_y into nitrates on dust particles during transport [156, 157]. Model studies have confirmed that the nitrate content is consistent with the uptake of reactive NO_y trace gases (such as HNO_3) [158]. The overall impact of NO_y-mineral aerosol interactions on tropospheric photochemical cycles has been assessed in combined aerosol/gas phase models [158–161]. They potentially impact mineral dust hydroscopic and optical properties, they change the gas phase composition (NO_y/NO_x ratio and ozone concentrations), and they establish a transport route of nitrate and sulfate to regions far from the sources (i.e., nitrogen fertilization of oceans) [162, 163]. The accuracy of the simulations is severely impacted by a lack of high quality laboratory data describing trace gas/dust interactions. As this section is focussing on dust photochemistry, the reader is referred to recent reviews on dust heterogeneous chemistry [164] for more information about the uptake of various gases on dust surfaces.

As dust particles are mobilised by strong winds and therefore eroded from the ground, their composition reflects the chemical composition of crustal materials from which they are produced. As the Earth's crust is dominated by silicon and aluminum oxides, the latter are also dominantly present in uplifted particles. Indeed, several studies focusing on the chemical (elemental) composition of dust originating from various locations around the world have demonstrated that mineral dust is approximately 60% SiO_2 and 10–15% Al_2O_3 (by weight) [165]. Beside these major elements, some other oxides are found. The percentages of these other oxides, namely Fe_2O_3, MgO, CaO, and TiO_2, are slightly more variable and dependent on source location. For instance, titanium dioxide is found in dust particles at mass mixing ratios ranging from 0.1% to 10% depending on the exact location from where the particles were uplifted [166].

Both titanium and iron oxides are known semiconductors used as photochemical sources of radicals (see Sect. 1). In aqueous solutions, iron oxides are used to induce the so-called Fenton or photo-Fenton reactions [167] (see section on bulk phase chemistry). Pure TiO_2 is used in a variety of remediation processes due to its photocatalytic properties. The exposure of TiO_2 to light with wavelengths below 400 nm leads to an electron hole pair. Each of these can reach the surface and react with adsorbed species to form OH, O_2^-, or singlet oxygen. These free-radicals are very efficient oxidizers of organic and inorganic matter. For instance, pure TiO_2 has been demonstrated in a number of studies to be an effective photocatalyst for NO_2 reduction [168–170]. Similar reactions also occur with other inorganic compounds such as ozone and sulfur oxides with synergistic effects being active if these

compounds are present in combination [171]. Accordingly, the TiO_2 contained in mineral dust could induce photochemical reactions that were not considered so far. In turn, this could drastically modify the chemistry of the dust particles and their potential impact on the tropospheric composition. As a consequence, there is a recent but growing interest in studies focussing on photochemical transformation at the air-dust interface. Several surface photochemical mechanisms are currently being discussed in the literature, i.e., surface photolysis and photo-assisted reactions.

The photolysis of nitrate on surfaces is especially important as it could lead to the renoxification of the atmosphere, whereby nitrate (or nitric acid) becomes a source of NO_x and thus mineral dust would not be a permanent sink for gaseous nitrogen oxides. uptake of several gases, i.e., NO_2 [126, 172, 173], O_3 [174], and HCHO [175], while [176] presented similar conclusion for the surface photooxidation of SO_2.

The striking features in all cases are that under illumination (1) the uptake of these gases is enhanced by more than one order of magnitude as compared to data obtained in the dark and (2) the reaction is sustained as long as light is available (while in the dark most surfaces are passivated in short time scales).

Let us focus on the case of nitrogen dioxide (NO_2) [126, 172, 173, 177], which is generally thought to be only very poorly reactive on a large variety of solid surfaces at room temperature and low gas phase concentrations. (We note that high concentrations may lead to the formation of N_2O_4 which, in turn, is known to be quite reactive on various surfaces [178].) However, once a dust surface is irradiated, in the range 300–400 nm and under conditions where gas phase photochemistry was shown to be minor (typically by the use of short reaction times), a very rapid chemical conversion of NO_2 is observed. Not only is the uptake rate drastically accelerated but it also appears that the uptake rate is catalytic in the sense that the uptake rate does not depend on time, i.e., no surface saturation has been observed on these synthetic samples over hours (even at NO_2 concentrations as large as 300 ppb). The uptake coefficients (normalized to the BET surface area) were observed to be close to 10^{-6}, up to two orders of magnitude larger than without light. Gustafsson et al. [179, 180] derived the uptake rate of NO_2 onto pure TiO_2 to be ca. 8×10^{-3}. Such photoenhancements were observed over a large range of dust surfaces including synthetic surrogates and samples originating from Mauritania, Algeria, Morocco, Tunisia, and Arizona (Arizona Test Dust, ATD); see Fig. 7. While the uptake in the dark was always very small, a photoenhanced uptake of NO_2 was observed on all samples with an enhancement factor ranging from 8 to 15.

The photocatalytic action of TiO_2 (and other semiconductors) is initiated by the photo-production of excess electrons in the conduction band (e^-_{cb}) and holes in the valence band (h^+_{vb}). The electron reduces the oxygen or the nitrogen dioxide while the hole oxidizes water vapor. The associated reactions mechanism could be [5]

$$\mathrm{Dust}(TiO_2) + h\nu \rightarrow h^+_{vb} + e^-_{cb} \tag{7}$$

$$h^+_{vb} + H_2O \rightarrow OH + H^+ \tag{8}$$

$$e^-_{cb} + O_2 \rightarrow O_2^- \tag{9}$$

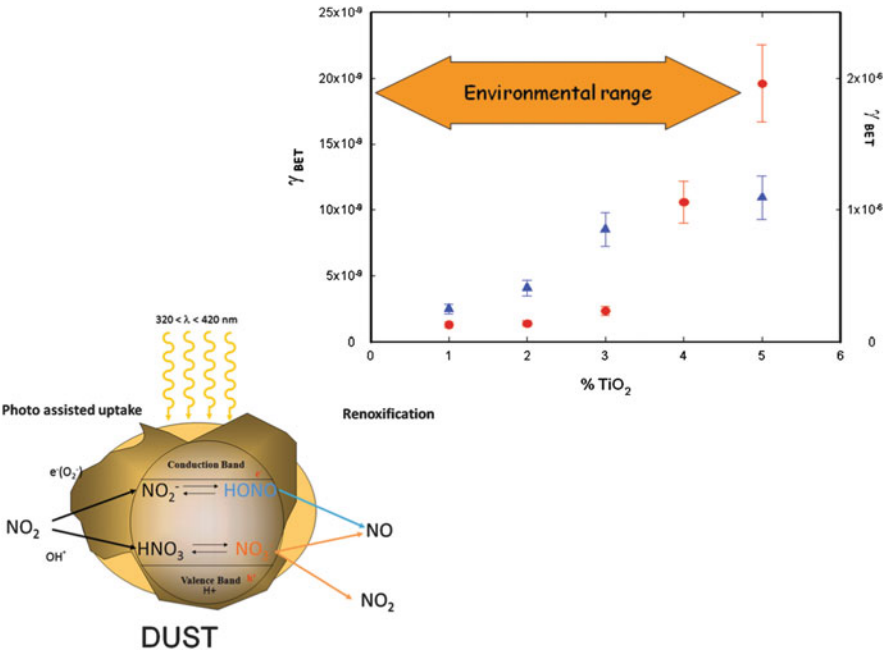

Fig. 7 Schematic representation of the conversion of NO_2 into HONO on UV-A (300–420 nm) irradiated mineral dust, illustrating the chemistry initiated by the photoinduced electron and hole, respectively. Dependence of the uptake coefficient (based on the BET surface) as a function of the TiO_2 content of synthetic dust

where OH and the electrons or O_2^-, respectively, can react with nitrogen dioxide according to

$$NO_2 + OH \rightarrow HNO_3 \tag{10}$$

$$NO_2 + O_2^- (\text{or } e^-_{cb}) \rightarrow NO_2^- + O_2 \tag{11}$$

It must be emphasized that these reactions are just a subset of a large number of possible reactions changing the final yield of each product. Depending on the acidity of the surface, the production of nitrite anions is linked to that of gaseous nitrous acid (HONO), known to be a very important source of hydroxyl radicals. HONO was observed from irradiated samples, but with varying yields. On synthetic dust surfaces (i.e., 1 wt% TiO_2 in SiO_2) HONO was produced with an average yield of 33% while, for an authentic Saharan sample, the yield was about 80%. This indicates that surface acidity, microstructure, and other factors finally control surface chemistry and the release of HONO.

It is well known that nitrate anions are formed as a consequence of the photocatalytic oxidation of NO_2 on UV-illuminated TiO_2 surfaces [181–186].

In addition, on the dust surface, nitrate anions were observed to be the only product formed during the photoconversion of NO_2. The formation of nitrate on dust particles is typically considered as a sink for atmospheric NO_y (such as HNO_3). However, if dust is photochemically or photocatalytically active, surface nitrate will photoreact according to

$$NO_3^- + h^+_{vb} \rightarrow NO_3 \tag{12}$$

$$NO_3 + h\nu \rightarrow NO + O_2 \tag{13}$$

$$NO_3 + h\nu \rightarrow NO_2 + O \tag{14}$$

The photocatalytic action of TiO_2 is again initiated by the photo-production of excess electrons in its conduction band (e^-_{cb}) and holes in its valence band (h^+_{vb}). The nitrate ion adsorbed at the oxide surface can react with the holes in the valence band to form a nitrate radical. The nitrate radical (NO_3), which absorbs strongly in the visible, can subsequently be photolyzed (occurring at longer wavelength compared to the anion) and form NO_2 and NO through reactions (13) and (14), respectively, as observed by Ndour et al., leading to a potential renoxification process of the atmosphere [177]. These processes are then in competition with surface photolysis as described by Grassian and co-workers [176, 187–189].

The latter two reactions above produce atomic and molecular oxygen that may lead to the formation of ozone at the surface. Monge et al. [129] investigated this chemical route by exposing a mix of TiO_2/KNO_3 50 wt% to near-UV irradiation (300–420 nm) using synthetic air or pure N_2 as carrier gases with 30% RH under atmospheric pressure and room temperature. The formation of ozone was indeed observed and explained by reactions (7) to (14) followed by a surface recombination:

$$O^\bullet + O_2 + M \rightarrow O_3 + M \tag{15}$$

Although O_3 has recently been proved to decompose on illuminated TiO_2 surfaces [174], its formation is observed when TiO_2 treated surfaces are exposed to NO_x under illumination. Charge transfer reactions take place at the surface of TiO_2, producing nitrate radicals from the corresponding anions. The photochemistry of the NO_3 radical leads to O_3 formation, enhancing the oxidizing power of these surfaces.

Recent laboratory work has shown that the uptake and photooxidation of organics on TiO_2-containing mineral dust proxies can be an efficient process [190]. *n*-Propyl and isopropyl alcohols were efficiently oxidized to propionaldehyde and acetone, respectively, after uptake to photoactive dust in a Knudsen cell reactor when the dust substrate was exposed to actinic radiation. The presence of trace amounts of O_2 in the reactor enhanced the production of oxidized product. These observations are consistent with the general mechanism for TiO_2 photoactivity, as shown below for isopropanol:

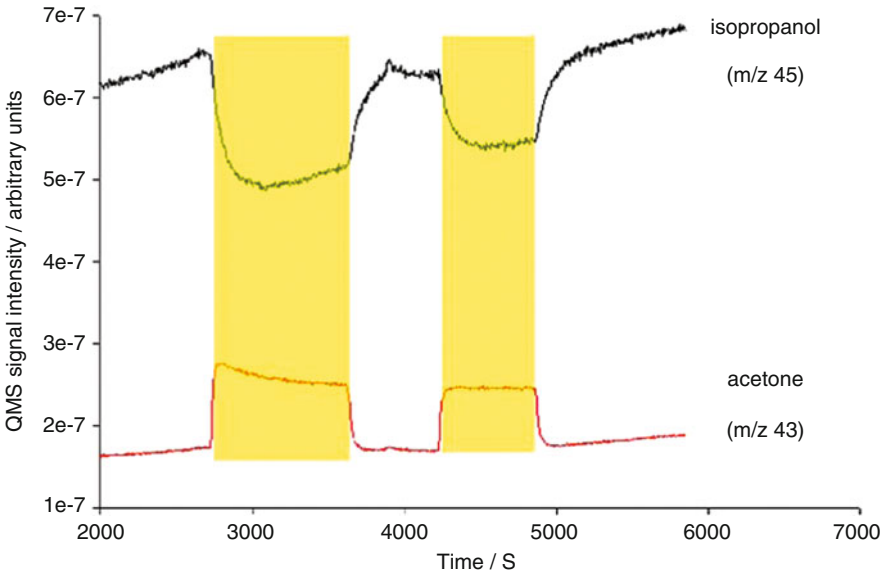

Fig. 8 Photoenhanced uptake of propanol and the corresponding production of acetone on an illuminated TiO_2 dust sample in the presence of 0.7 Pa of O_2(g)

$$h^+_{vb} + (CH_3)_2CHOH \quad \rightarrow\rightarrow \quad (CH_3)_2CO \tag{16}$$

$$\{>TiOH^{\bullet}\}^+ + (CH_3)_2CHOH \rightarrow\rightarrow (CH_3)_2CO \tag{17}$$

$$O_2^{-\bullet} + (CH_3)_2CHOH \rightarrow\rightarrow (CH_3)_2CO \tag{18}$$

Figure 8 displays the photoenhanced uptake of propanol and the corresponding production of acetone on an illuminated TiO_2 dust sample in the presence of 0.7 Pa of O_2(g).

4 Tropospheric Aqueous Phase Bulk Photochemistry

4.1 Introduction

Atmospheric particles very often contain water when they occur as deliquesced aerosol particles, haze, fog, cloud droplets, or even rain droplets (hydrometeors). It has been suggested before that the atmospheric aqueous bulk phase in these systems might also host a lively and important photochemistry which, up to now, has mostly been described insofar as hydroxyl (OH) radicals are generated by the photolysis of nitrate, nitrite, hydrogen peroxide [191–198], and iron-hydroxyl complexes [199]. These processes have been treated in recent overviews such as [200, 201].

Photosensitization has been studied not only in connection with interfaces but also for bulk phase aqueous environmental systems [202].

Iron is the most abundant metal in the Earth's crust and is always identified as a component in tropospheric particle systems, either aqueous or dry [167]. It has been known for a long time that iron forms chelate complexes very efficiently and that oxalate forms complexes with Fe(III). These can be regarded as being very stable from their complex stability constants but they also exhibit a considerable potential for light absorption in the actinic range of the spectrum. Iron-oxalato-complexes have been characterized with regard to their photochemical activity by the measurement of their effective quantum yields for the formation of Fe(II) [203, 204]. As a consequence of this chemistry the formation of iron-oxalate complexes is included in the series of CAPRAM (Chemical Aqueous Phase Radical Mechanism) schemes for atmospheric aqueous phase chemistry [205]. Leaving these very important photochemical sink processes out of any description of tropospheric aqueous phase chemistry results in a dramatic overestimation of aqueous phase oxalate formation and, as a consequence, gives rise to misleading interpretations. Below, we discuss the molecular mechanisms underlying bulk aqueous phase photochemistry of the iron-oxalato-complexes and present an introduction to the study of other Fe(III) complex systems. There are strong interactions among the photochemically generated radical species formed in complex photolysis reactions. We further discuss the possible impacts of extending the iron complex photochemistry treatment in tropospheric chemistry simulations. Such impacts include, for example, the formation of Fe(II) in aqueous phase photochemical redox-cycling and the degradation of dissolved organics which may be "activated" by complexation to iron centers.

4.2 Ferrioxalate Photochemistry

Ferrioxalate complexes are thought to hold a major portion of Fe(III) in atmospheric waters [167]. Although such complexes are widely used as chemical actinometers [206] and have been the subject of numerous experimental investigations [207–218], the exact primary step in ferrioxalate photochemistry is still controversial. Two different versions of the ferrioxalate reaction mechanism have been proposed following the excitation of the complex [219]. One possibility is an intramolecular electron transfer from the oxalate ligand to the center ion Fe(III) and the formation of a long lived radical complex (19) or the formation of a $C_2O_4^{\bullet -}$ radical (20) [213, 215]:

$$[Fe^{(III)}(C_2O_4)_3]^{3-} + h\nu \rightarrow [Fe^{(II)}(C_2O_4^{\bullet})(C_2O_4)_2]^{3-} \quad \text{or} \tag{19}$$

$$\rightarrow [Fe^{(II)}(C_2O_4)_2]^{2-} + C_2O_4^{\bullet -} \tag{20}$$

The $C_2O_4^{\bullet -}$ radical will then decarboxylate instantly and form CO_2 and $CO_2^{\bullet -}$ [220]:

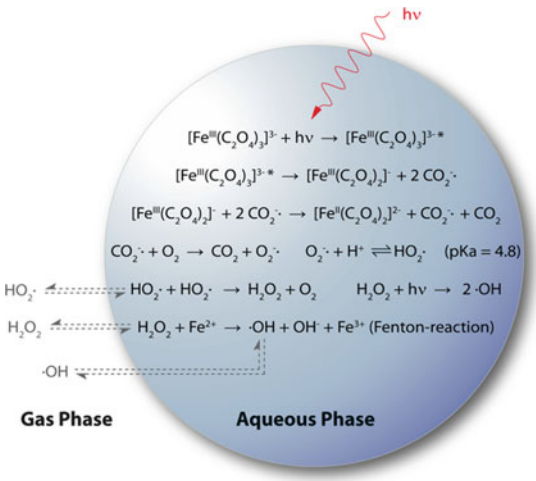

Fig. 9 Photolysis of Fe(III)-oxalato complex in the atmospheric aqueous phase, including subsequent reactions and possible interactions with the gas phase

$$C_2O_4^{\bullet -} \rightarrow CO_2^{\bullet -} + CO_2 \quad k_{1st} = 2 \times 10^6\ s^{-1} \tag{21}$$

Another option is the sequential cleavage of the Fe(III)–O bond between iron and one oxalate ligand and its C–C bond which produces a biradical complex or two $CO_2^{\bullet -}$ radicals [211, 216, 221]:

$$\left[Fe^{(III)}(C_2O_4)_3\right]^{3-} + h\nu \rightarrow \left[Fe^{(III)}(CO_2^{\bullet})_2(C_2O_4)_2\right]^{3-} \quad \text{or} \tag{22}$$

$$\rightarrow \left[Fe^{(III)}(C_2O_4)_2\right]^{-} + 2CO_2^{\bullet -} \tag{23}$$

The different proposed mechanisms were presented by two research groups; [219, 222, 223], both groups presenting experimental evidence for their findings. Thus, it might be possible that both reaction mechanisms take place simultaneously depending on parameters such as mono-, bis-, or tris-oxalato coordination, excitation wavelength, or excitation energy. In atmospheric aqueous phases chemistry it is of importance which mechanism holds; that is, whether one Fe(II) and one $CO_2^{\bullet -}$ or two $CO_2^{\bullet -}$ radicals are produced. $CO_2^{\bullet -}$ is capable of producing Fe(II) via secondary reactions with parent Fe(III)-oxalato complexes but can also react with other electron acceptors such as O_2 which are likely to compete in more or less dilute atmospheric aqueous media (Fig. 9). Regardless of the exact reaction mechanism, the ferrioxalate system can produce Fe(II) quantum yields larger than unity because of the secondary Fe-reduction by the $CO_2^{\bullet -}$ radical formed.

Figure 9 illustrates the complicated interactions of iron-oxalato complex photochemistry with radical chemistry and the chemistry of organic substances. The main impacts of iron complex photochemistry are ultimately (1) breaking of C–C bonds and thus degradation of the ligand (oxalate) and (2) formation of radicals

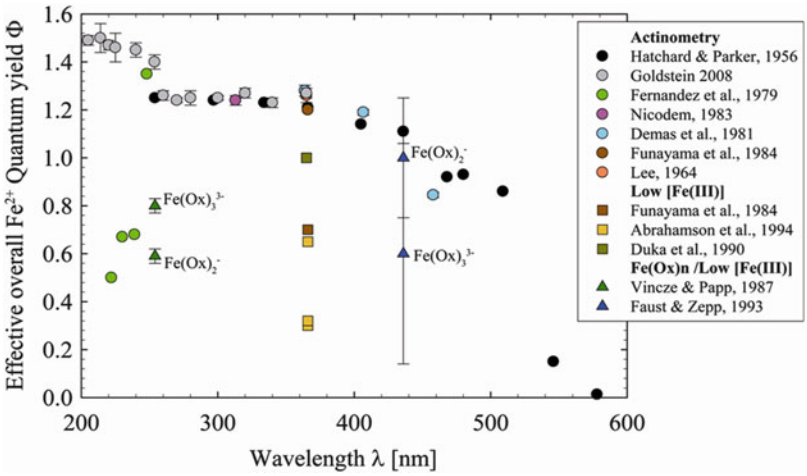

Fig. 10 Overview of Fe^{2+} quantum yield measurements in argon saturated solutions for the ferrioxalate system, Actinometry: specified actinometry conditions, high initial Fe, [Fe(III)] = 0.006–0.15 M, 0.05 M H_2SO_4, see Hatchard and Parker [206] for details; low [Fe(III)]: lower initial Fe(III) concentrations than actinometry conditions, Fe(Ox)n: individual complexes

which can lead to turnover of substances present in the droplets or deliquesced particles.

A prerequisite to simulate the impact of iron complex photochemistry in atmospheric aqueous systems is the characterization of its efficiency. Figure 10 presents an overview of quantum yield measurements in the ferrioxalate system as a function of wavelength.

At first glance, the results appear quite scattered. The values obtained under conditions of chemical ferrioxalate actinometry represent the upper boundary of the reported values, which mostly agree with each other. Between 250 and 350 nm the quantum yields are fairly constant around $\Phi \sim 1.25$. Ferrioxalate actinometry is performed under standardized conditions using millimolar concentrations of ferrioxalate (and above millimolar at $\lambda \geq 436$ nm) and an acidic pH (0.05 M H_2SO_4) of about 1.2 [206]. Other measurements have been carried out at lower initial Fe(III) concentrations as well as different Fe(III) to oxalate ratios and different pH values; these mostly result in lower Fe(II)-quantum yields. Some investigations discriminating between individual complexes of Fe(III) and oxalate have been performed, while others did not provide an analysis of the individual complexes and are thus valid only for their respective complex-mixtures. However, all measurements with initial Fe(III) concentrations below millimolar result in lower quantum yields. It is therefore desirable to characterize systemically any possible effects of initial Fe(III) complex concentration, speciation, and other experimental conditions on the ferrioxalate quantum yield to be able to interpret reported differences.

At initial Fe(III) concentrations higher than 2×10^{-4} M, quantum yields of $\Phi \sim 1.25$ are obtained using 308-nm laser flash photolysis, in agreement with the

values measured under actinometry conditions [204]. At lower initial Fe(III) concentrations the measured quantum yields begin to decrease down to approximately half of the maximum value. This phenomenon can be explained by a kinetic effect of the concentration decrease on the secondary reactions involved in Fe(II) formation. The recombination of $CO_2^{\bullet-}$ radicals to form oxalate becomes more favored at more dilute conditions whereas the secondary reduction of unphotolyzed Fe(III) species by $CO_2^{\bullet-}$ becomes less effective at lower Fe(III) concentrations. These findings can explain the discrepancies between measured ferrioxalate quantum yields (Fig. 10) and should be considered when ferrioxalate photochemistry takes place at sub-millimolar initial concentrations.

4.3 Photochemistry of Fe(III) Polycarboxylate Complexes

As discussed above, the first step in photochemical reactions of Fe(III) carboxylate complexes has been thought to involve ligand to metal charge transfer [224, 225] as a concerted inner sphere electron transfer, and the subsequent separation of the photofragments into the bulk solution. It can be written in simplified form as

$$[Fe^{(III)}(OOC\text{-}R)]^* \rightarrow Fe^{2+} + R\text{-}COO^{\bullet} \tag{24}$$

where $R\text{-}COO^-$ is the carboxylate ligand and $R\text{-}COO^{\bullet}$ is the primary organic radical formed. Recently, investigations of the primary photochemical steps in polycarboxylate complex photochemistry have been carried out using time resolved transient spectroscopy. These investigations report the formation of long lived radical complexes (25) with lifetimes in the millisecond range as the main reaction path (90–98% of photoactivated complexes) whereas (24) only accounts for 2–10% decay of photoactivated complexes [226–230]:

$$[Fe^{(III)}(OOC\text{-}R)]^* \rightarrow [Fe^{(II)}(^{\bullet}COO\text{-}R)] \tag{25}$$

$$[Fe^{(II)}(^{\bullet}OOC\text{-}R)] \rightarrow Fe^{2+} + {}^{\bullet}OOC\text{-}R \tag{26}$$

However, it could be argued that, despite the discovery of the new transient, the net chemical products are identical with those in (24). Possible reactions of the long lived radical complex are poorly characterized but they will most likely influence the quantum yield and product formation depending on the reaction conditions and available reaction partners. In laboratory systems such reactions could involve dissolved O_2, other Fe(III) species, or back-electron transfer; reaction paths in the atmospheric aqueous phase would be less restricted.

After the radical complex decays, $R\text{-}COO^{\bullet}$ will decarboxylate instantaneously ($k_{R27} \sim 10^9$–$10^{12}\ s^{-1}$) [231–233]:

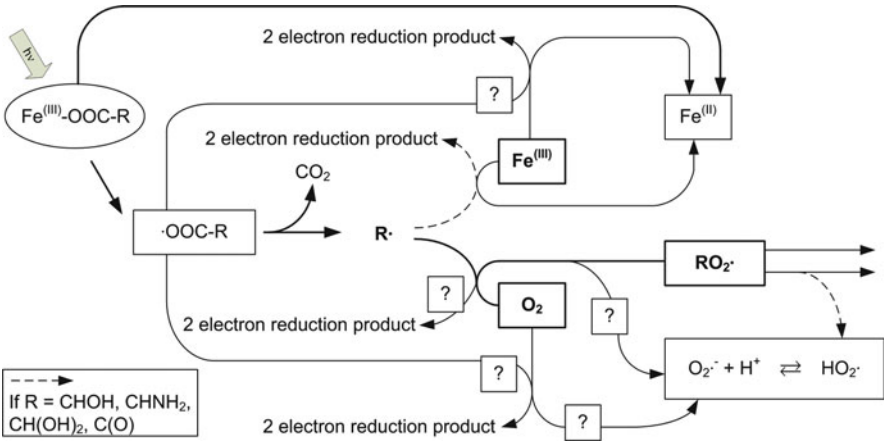

Fig. 11 Scheme of Fe(III) complex photochemistry, modified after [203], 2 electron reduction can only occur in case of hydroxyl, amino, diol, or keto substitution at the radical bearing C-atom; questionable and rather improbable reaction paths have been marked with ?, see text for discussion

$$\text{R-COO}^{\bullet} \rightarrow \text{R}^{\bullet} + \text{CO}_2 \tag{27}$$

followed by the rapid reaction of the alkyl radical $R^{\bullet}$ with dissolved oxygen, forming a peroxyl radical with $k_{R28} \sim 2 \times 10^9\ M^{-1}\ s^{-1}$ [234]:

$$\text{R}^{\bullet} + \text{O}_2 \rightarrow \text{RO}_2^{\bullet} \tag{28}$$

Subsequent reactions of $R^{\bullet}$ and $RO_2^{\bullet}$ can be specific depending on the type of ligand and its substitution. The scheme in Fig. 11 presents a critical evaluation of possible reactions following complex photolysis proposed by Faust and Zepp (1993). The main channels are electron transfer reactions of the alkyl radical $R^{\bullet}$ with Fe(III) species and the formation of peroxyl radicals $RO_2^{\bullet}$.

It should be noted that the formation of peroxyl radicals seems to be the most favourable path, because dissolved O_2 is present in concentrations of around 3×10^{-4} M at atmospheric pressure and (28) is usually fast ($k_{R28} \sim 2 \times 10^9\ M^{-1}\ s^{-1}$ [234]). Furthermore, an electron transfer reaction of the alkyl radical $R^{\bullet}$ with Fe(III) or O_2 seems to be feasible only if there is a hydroxyl, amino, diol, or keto substitution on the radical bearing C atom [235, 236]. Unfortunately, the pathway of an electron transfer reaction of the alkyl radical $R^{\bullet}$ with O_2 forming $O_2^{\bullet -}$ has been postulated as a general pathway following Fe(III)-organic complex photolysis by a number of authors [167, 224, 237–241]. This is overly simplified and can be misleading, since a mechanism can only be explained in the case of hydroxyl-, amino-, diol-, or keto-substitution. It has to be emphasized that the peroxyl radical formation is expected to be a major reaction route after Fe(III) organic complex photolysis other than oxalate for the above-mentioned reasons.

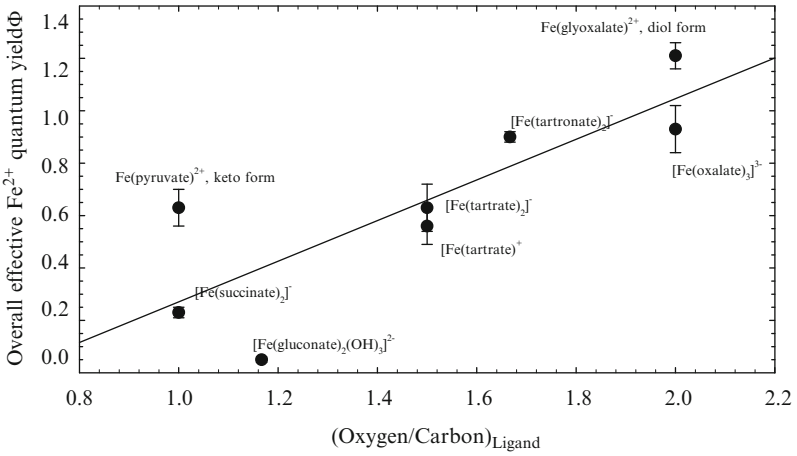

Fig. 12 Measured overall Fe^{2+} quantum yields of Fe(III) complexes as function of oxygen to carbon ratio of the ligand (308 nm single flash photolysis, Ar saturated solutions)

Peroxyl radical formation has been suggested, for example, in the photolysis of Fe (III) acetate [242] and Fe(III) malate [243]. According to the known pathways of peroxyl radical chemistry in solution [234], formation of H_2O_2, $HO_2^{\bullet}$, and stable organic end products will occur. Consequently, $O_2^{\bullet-}$ can be produced indirectly via $HO_2^{\bullet}$ elimination in some cases.

Fe^{2+} quantum yield measurements of several other atmospherically relevant Fe(III) carboxylate complexes have been performed for excimer laser flash photolysis [204, 227] and Hg(Xe) lamp photolysis [203, 235, 244, 245]. Different experimental types of quantum yield determinations have been listed. Quantum yields labelled with ΦFe(II) Ar are Fe(II) quantum yield measurements in argon saturated solution, while those labeled ΦFe(II) O_2 pertain to Fe(II) quantum yield measurement in solutions saturated with atmospheric oxygen. For ΦFe(III) the initial Fe(III) complex disappearance upon photolysis was measured. In the case of Φmalonate the amount of the malonate ligand that was photochemically decomposed was measured, leading to a ligand disappearance quantum yield. The range of measured quantum yields among the different carboxylate ligand complexes with Fe^{3+} shows a large variability with measured Fe^{2+} quantum yields from 0.021 to 1.21 at the chosen reference wavelength 308 nm (Fig. 12).

Obviously, the choice of ligand seems to affect the measured quantum yields. A trend of increasing overall Fe(III) quantum yields of Fe(III) complexes with increasing oxygen to carbon ratio of the ligands is seen among the investigated complexes (Fig. 12).

Oxygen can be present in three different binding modes in the carboxylates considered here: the carboxylate, hydroxyl, and keto groups. Additionally, the keto-form can be hydrated, forming a gem-diol with two hydroxyl groups at one carbon atom. Oxygen substitution is thought to affect the photoreactivity in two ways. The first is via inductive effects causing better ligand-to-metal charge transfer (LMCT) in the primary reaction step, as explained for glyoxalate and

pyruvate above. It is presumed that the increased electron density through the oxygen lone electron pairs of the -OH, -C(O)-, or -$CH(OH)_2$ groups can be inductively propagated to the neighboring -COO^- group, thus facilitating the LMCT. Second, the influence can occur via the presence of an oxygen containing group on the C-atom next to the LMCT-involved carboxylate group, which enables a two electron oxidation product of the ligand. Ligand fragments, which are able to undergo a two electron oxidation after decarboxylation, are those of tartronate and tartrate (both $^{\bullet}$CHOH-R), pyruvate ($^{\bullet}$C(O)-R), and glyoxalate ($^{\bullet}CH(OH)_2$). The unpaired electron can be transferred to parent Fe(III) complexes and thus increase the Fe(II) yield. Additionally, the peroxyl radicals formed from ligand fragments of tartronate, tartrate, and glyoxalate can undergo an $HO_2^{\bullet}$ elimination, which can further cause secondary Fe(II) production.

Fe(III) complexes having a primary organic fragment after decarboxylation with $^{\bullet}CH_2$-R structure (such as complexes of malonate, succinate, and glutarate) all display significantly lower quantum yields compared to the more oxygenated compounds discussed above (Fig. 12). With the $^{\bullet}CH_2$-R structure, a second electron oxidation step of the ligand is not possible; instead the fragments can only decay through peroxyl radical formation and subsequent recombination. Thus no relevant secondary Fe(II) production occurs in systems with $^{\bullet}CH_2$-R structure, and observed quantum yields are accordingly low. An additional factor causing low Fe(II) quantum yields in the case of malonate is the reported quenching mechanism with a free ligand that causes reoxidation of Fe(II) [245]. Quenching was also reported for Cu(II) malonate photolysis, but not for Cu(II) complexes with succinate and glutarate [246].

In the presence of dissolved O_2, peroxyl radicals $RO_2^{\bullet}$ can form in the reaction of photochemically produced alkyl radicals $R^{\bullet}$. Generally, oxygen has the effect of decreasing the quantum yield (Table 1). This is usually attributed to the secondary production of oxidants such as H_2O_2, $O_2^{\bullet-}/HO_2^{\bullet}$, and $RO_2^{\bullet}$ [203, 230]. The radical species $O_2^{\bullet-}/HO_2^{\bullet}$ can act as both oxidizing and reducing agents. According to a kinetic reaction simulation of the Fe(III) glyoxalate system, the measured effects of lower quantum yields in the presence of dissolved O_2 could not be reproduced with the simulation, despite using sensitivity test runs focusing on reaction paths that are sensitive to O_2 [204]. Consequently, the O_2 effect cannot be kinetically simulated and thus our knowledge about Fe(III) photochemical processes is not complete in this respect. The causes of a quantum yield decrease seem to be complex and therefore the O_2 effect has to be considered separately for each system.

4.4 Atmospheric Chemistry Simulation with Extended Fe(III) Complex Photochemistry in CAPRAM

The binding of Fe in different complex species is determined by the amount of potential ligands present, their respective stability constants and the pH. Due to the high stability constants and being a major fraction of organic compounds in the atmospheric liquid phase, mono- and dicarboxylic acids are among the most

Table 1 Summary of quantum yield measurements from Fe(III) carboxylate complex photolysis at different wavelengths using laser flash or continuous Hg(Xe) lamp irradiation

Ligand/complex	Experiment type	Flash photolysis 308 nm	Flash photolysis 355 nm[a]	Lamp photolysis 365/366 nm	Lamp photolysis 436 nm
Oxalate					
$[Fe(OOCCOO)_2]^-$	$\Phi_{Fe(II)}$ Ar	[b]			**1.40 ± 0.40** 1.00 ± 0.25[c]
$[Fe(OOCCOO)_3]^{3-}$	$\Phi_{Fe(II)}$ Ar	**0.93 ± 0.09**			**1.00 ± 0.20** 0.60 ± 0.46[c]
Malonate					
$[Fe(OOCCH_2COO)_2]^-$	$\Phi_{malonate}$ $\Phi_{Fe(II)}$ Ar			0.036 ± 0.005[d] 0.027[c] 0.0074 ± 0.0008[d]	
Tartronate					
$[Fe(OOCCHOHCOO)_2]^-$	$\Phi_{Fe(II)}$ Ar	**0.90 ± 0.02**		0.50[e]	
Succinate					
$[Fe(OOC(CH_2)COO)_2]^-$	$\Phi_{Fe(II)}$ Ar	**0.23 ± 0.02**		0.13[f]	
Tartrate	$\Phi_{Fe(III)}$		0.47		
$Fe(OOC(CHOH)_2COO)^+$	$\Phi_{Fe(II)}$ O_2		0.40		
	$\Phi_{Fe(II)}$ Ar	**0.56 ± 0.07**	0.44	0.42[e] 0.40 (pH 2.7)[f]	
$[Fe(OOC(CHOH)_2COO)_2]^-$					
	$\Phi_{Fe(II)}$ Ar	**0.63 ± 0.09**		0.58 (pH 4)[f]	
Pyruvate	$\Phi_{Fe(III)}$		0.53		
$FeOOCCOCH_3^{2+}$	$\Phi_{Fe(II)}$ O_2	**0.47 ± 0.07**	0.46		
	$\Phi_{Fe(II)}$ Ar	**0.63 ± 0.07**	1.00		
Glyoxalate	$\Phi_{Fe(III)}$		0.70		
$FeOOCC(OH)_2^{2+}$	$\Phi_{Fe(II)}$ O_2	**0.76 ± 0.05**	0.80		
	$\Phi_{Fe(II)}$ Ar	**1.21 ± 0.05**	1.05	0.97[e]	
Gluconate					
$[Fe(HOCH_2(CHOH)_4COO)_2(OH)_3]^{2-}$	$\Phi_{Fe(II)}$ Ar	**0.05 ± 0.01**			

ΦFe(II) Ar is Fe(II) quantum yield measurement in Ar saturated solution, ΦFe(II) O_2 is Fe(II) quantum yield measurement in atmospheric oxygen saturated solution, ΦFe(III) is initial Fe(III) complex disappearance quantum yield, Φmalonate is ligand disappearance quantum yield

Bold values: [204]

[a][227]

[b]Not determined due to experimental limitations

[c][203]

[d][245], 300–366 nm integral

[e][244]

[f][235]

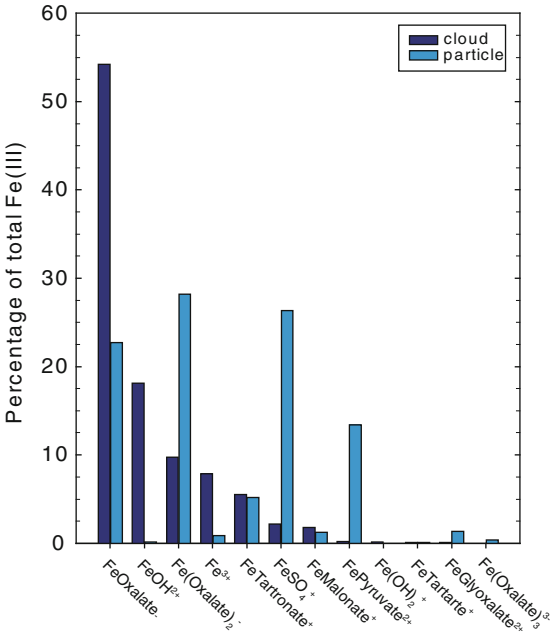

Fig. 13 Fe(III) speciation in cloud water and wet particles when included in the chemical aqueous phase radical mechanism (CAPRAM) to simulate aqueous tropospheric chemistry

important ligands for Fe to be considered [167, 247]. Realistic speciation calculations have been performed using a set of iron complex reactions based on kinetics implemented in the CAPRAM [248], which contains organic chemistry up to C4 compounds.

The major fraction of Fe(III) is bound in carboxylate complexes, mainly with oxalate, and a smaller fraction in inorganic complexes with hydroxide and sulfate in both scenarios, cloud and deliquesced particles (Fig. 13). After oxalate, complexes with tartronate, pyruvate, malonate, and glyoxalate altogether constitute a significant portion of the total soluble Fe(III). It is important to distinguish cloud and particle periods because the differences in pH ($pH_{cloud} = 3.2$, $pH_{particle} = 1.2$) and liquid water content (LWC) lead to a largely different Fe(III) species distribution. Other calculations with an equilibrium speciation model show that complexes with tartrate, lactate, and malate may also be able to compete with the aforementioned carboxylates when their concentrations approach the upper limit that has been reported for cloud water or ambient particles. Since oxalate complexes constitute the largest fraction of bound Fe(III), their photochemistry is especially interesting.

Iron complex photolysis is one of the processes that produce reduced iron (Fe(II)) in a highly oxidizing environment like the atmospheric aqueous phase. There are numerous other processes such as reactions with HO_x species or Cu(I)/Cu(II) which can reduce or oxidize iron in the troposphere. These reactions can take place simultaneously and cause iron to undergo a so-called redox-cycling [167]. Because of the large number of complex interactions in the atmospheric chemistry of the transition metal iron, it is useful to utilize models to assess the impact of the complex iron photochemistry.

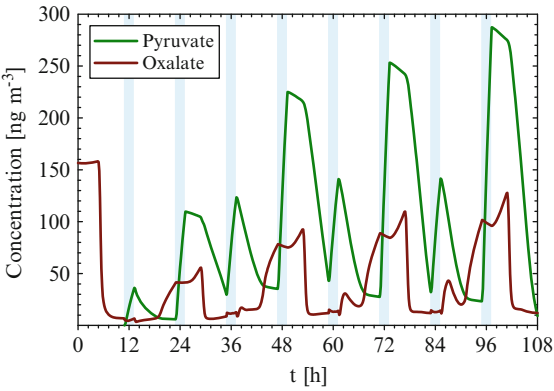

Fig. 14 Simulated concentration time profiles for the Fe(III) ligands pyruvate and oxalate, summation of all forms of the respective ligand (free mono- or di-anion, free acid and ligand bound in Fe(III)-complexes), light blue stripes indicate cloud periods, in between are wet particle periods

Photolysis reactions of Fe(III) complexes with malonate, tartronate, succinate, tartrate, and glyoxalate were implemented in CAPRAM; Tilgner and Herrmann [248]) as "extended Fe-carboxylate photochemistry." The former version of CAPRAM contained only Fe-sulfato, Fe-hydroxyl, and Fe-oxalato complex photochemistry. CAPRAM as part of the SPectral Aerosol Cloud Chemistry Interaction Model (SPACCIM [249]) has been applied in a 4.5-day non-permanent cloud simulation including 8 cloud passages between deliquescent particle periods. Fe (III) complex photolysis represented a small contribution to oxidant formation, where 1.3% of the total $O_2^{\bullet-}/HO_2^{\bullet}$ aqueous phase daytime sources in the model could be directly attributed to complex photolysis. Because Fe(III) complex photolysis can only occur during the daytime, only the daytime source fluxes have been considered. For this comparison, the daytime flux values of each reaction channel contributing to $O_2^{\bullet-}/HO_2^{\bullet}$ production were averaged over the entire simulation time of 108 h and added to give the 100% reference. $O_2^{\bullet-}/HO_2^{\bullet}$ contributing channels for the aqueous phase are in situ decay reactions of peroxyl radicals formed via oxidation processes, but the largest source is phase transfer from the gas phase. The contribution of Fe(III) complex photoreduction to the average Fe(II) formation flux over the total simulation time was 7% from Fe(III) oxalato complex photolysis, and 1% from additionally implemented other Fe(III) carboxylato photolysis reactions. Additional sources of reduced iron were reactions with $O_2^{\bullet-}/HO_2^{\bullet}$ and reactions with copper. The Fe(III) complex photolysis reactions can be a major sink for the carboxylate species besides radical reactions of OH, NO_3, or SO_4^{-}. Almost the entire oxalate in the simulation is depleted through Fe(III) complex photolysis, whereas 40% of the simulated pyruvate was degraded via complex photolysis and the remaining 60% via radical reactions. Percentage values here refer to averaged sink fluxes over the total simulation time.

Figure 14 shows simulated concentration time profiles for the Fe(III) ligands pyruvate and oxalate, which have mostly lower concentrations during the daytime, when the photochemistry as described here is active. Thus, it has to be emphasized that Fe(III) complex photolysis reactions can be a major sink for the carboxylate species besides radical reactions, and it is crucial not to neglect these reactions when the fate of carboxylic acids in the atmospheric aqueous phase is considered.

5 Photochemistry Associated with Ice

Ice is an abundant material found in the environment in the form of ice particles in the atmosphere, sea ice on oceans, and snow and glaciers on the continents. The surface of ice in each of these compartments is more or less continuously exposed to the atmosphere. Thus potentially a continuous exchange in both directions of atmospheric trace gases with these ice surfaces exists. The general role of environmental and atmospheric ices in affecting the oxidative capacity of the atmosphere, the biogeochemistry of short and long-lived organic pollutants, the cycling of halogen gases, and the nitrogen oxide cycle has been reviewed recently [250–253]. Those parts of environmental ice that are in direct contact with the atmosphere and thus the most relevant parts also experience irradiation by the sun. The illuminated, or photic, zone in snow packs in alpine or polar environments constitutes a significant fraction of those parts of snow or firn that exchange with the overlying air [254–256]. Similar arguments may hold for sea ice. The vanishingly small absorption cross section for water in the visible and near UV regions of the spectrum means that photochemistry in ice is governed by the presence of chromophoric material there. One example of processes induced by chromophoric material in snow is illustrated in Fig. 15 showing the emission of HONO from snow containing humic material exposed to NO_2 and UVA light, which will be discussed further below.

Ice itself is a high temperature material in the sense that under environmental conditions it is close to its melting point. The relatively weak hydrogen bonds which are the basis for the crystalline solid (hexagonal Ih ice) allow the surface to become disordered in response to the broken symmetry near the surface [258]. This disordered layer is a general surface phenomenon of solid matter and also referred to as surface premelting or quasi-liquid layer (QLL) [259] and involves the top few nanometers near the surface. This layer may present a particular environment for adsorbing trace gases, which may exist there with a local environment different from that in a liquid or solid solution. Atmospheric ice particles nucleate from solution droplets or on refractory material so that most of them remain with some solutes left as solution pockets in equilibrium with ice or attached dust or carbonaceous material [260]. Those solution pockets must not be confused with the QLL as they are considered a thermodynamically stable phase [261]. This microstructure determines the specific environment for photochemical processes with ice in the atmosphere, but also with snow derived from this ice. Once precipitated, snow continuously changes its microstructure through metamorphosis [262–264] that may lead again to relocation of associated material. The snow structure is also crucial to determine the depths to which radiation reaches in the actinic wavelength region [265]. Sea ice presents a polycrystalline structure with the solutes present within a brine solution in cracks, veins, and triple junctions, or also on the surface [266–269], out of which frost flowers may grow [270].

In the following paragraphs we will summarize the recent developments in understanding direct and indirect photochemical processes in the “light” of this

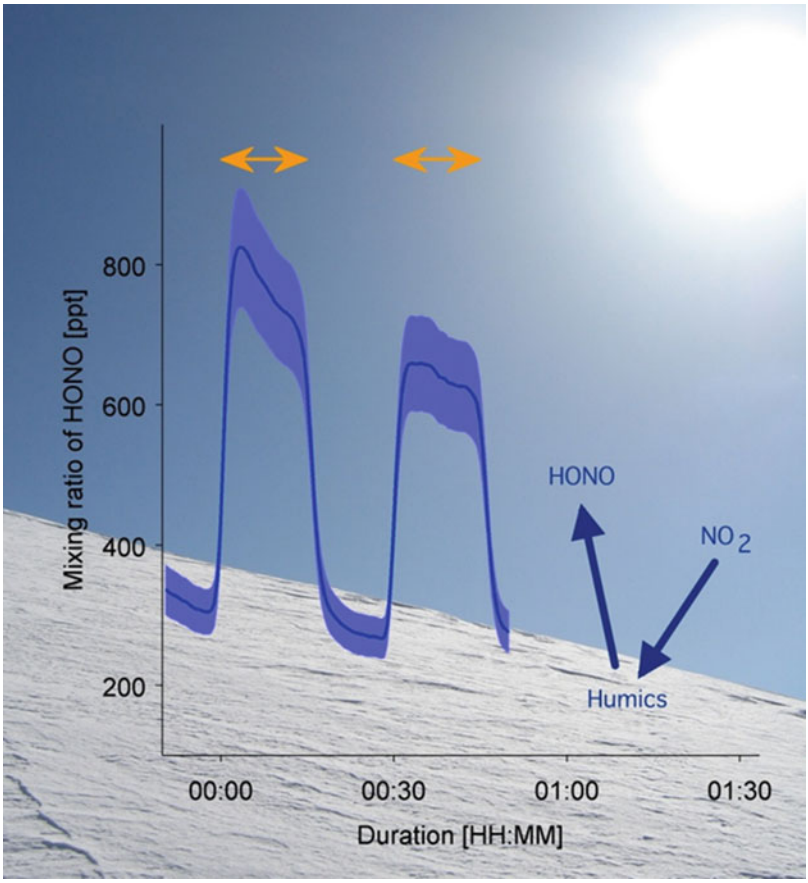

Fig. 15 Evolution of the HONO gas phase mixing ratio (*solid line*) with time after contact of NO_2 with humic acid doped ice. Two consecutive irradiation periods in the visible range (*orange arrows*) in the presence of NO_2 in the gas phase are shown. The *shaded area* illustrates the accuracy of the HONO measurement. Time zero denotes the beginning of the (first) irradiation period [257]

structural picture of ice in the environment [367]. The examples include organic and inorganic chromophores as far as they are implicated in the chemistry of atmospherically relevant gases.

The general significance of photochemical processes in snowpacks has been reviewed by Grannas et al. [251]. Evidence has emerged that many insoluble and soluble organic compounds are associated with ice in snow that may be responsible for a wealth of direct and indirect photochemical processes [271]. While many direct photolytic processes have been considered in the past [251], indirect processes, especially those involving organic chromophores, have only been recognized in this context recently. As an example, Rowland et al. [255] demonstrate that organic and inorganic chromophores induce photochemical degradation

of aldrin and dieldrin in frozen aqueous solutions. They also argue that the specific arrangement of soluble chromophores and the hydrophobic target leads to distinctly different degradation behavior compared to that in solution.

Almost all laboratory studies of ice photochemistry have used illuminated bulk ice samples, with reagents frozen in solution. Often it is assumed that the reagents are excluded together and uniformly to the ice surface region in contact with the overlying atmosphere. Various thermodynamic formulations have been used to estimate the concentrations of the excluded reagents [272, 273], but such approaches seem to be deficient in some cases [274]. Nevertheless, photolytic kinetics experiments have generally, but not always, found similar loss rates for species frozen from solution as in the liquid phase [192, 251, 275–277].

Recently it has become possible to test the assumption that photochemistry of compounds present at the air-ice interface, whether through exclusion during freezing or following deposition from the gas phase, is well described by the corresponding solution-phase process. Donaldson and co-workers have used glancing-angle laser fluorescence and Raman spectroscopy to probe chemical processes at the condensed phase-air interface of water and ice surfaces [93, 278–280]. They report that at least in the case of aromatic organic compounds, photolysis on "pure" ice surfaces is significantly faster than on liquid surfaces or that occurring within the ice matrix. This is a true surface effect, as demonstrated by experiments in which the photolysis rate is seen to be directly related to the surface/volume ratio of the ice [281]. Another study altered the surface properties of the air-ice interface, by freezing salt solutions such that an increasing amount of a "quasi-brine-layer" was present at the interface [281]. The photolysis rate of an aromatic test molecule at the air interface became slower as that interface became more "liquid-like" on a microscopic level, until it became identical with the rate seen on a liquid surface. This result also showed that increased light scattering at the ice vs liquid surfaces (or within the ice matrix) is not responsible for the enhanced photolysis rates.

One possible reason for this rate enhancement, at least in some instances, is a change in absorption cross sections and/or photolysis quantum yields due to self-association at the interface. This effect has been documented for aromatic compounds both spectroscopically and by simulations [278, 282, 283], and is a consequence of the different hydrogen bonding environment present at the air-ice interface compared to the liquid surface. In the case of benzene in particular, the self association gives rise to a significant red-shift in the absorption spectrum [279], such that benzene present at the air-ice interface may absorb available solar radiation in the lower atmosphere. This opens the possibility of a previously unconsidered fate for several aromatic pollutants present in snow- and ice-covered regions.

The majority of the examples mentioned above are concerned with oxidative degradation processes. Bartels-Rausch et al. [257] have shown that organic chromophores in ice can also reduce atmospheric gases. Humic acid was demonstrated to reduce nitrogen dioxide to gaseous nitrous acid, and this reaction was further found to be significantly enhanced by visible light. It was argued that organic sensitizers, such as benzophenone, receive an electron from a donor, such

as phenols, upon irradiation and pass this electron to NO_2 [127, 128, 202]. Both benzophenone and phenols represent typical building blocks of humic matter and have also been identified in polar surface snow [251]. Recent HONO emission measurements at Barrow, Alaska indeed indicated that this process is responsible for light induced HONO production during the day [284]. Bartels-Rausch et al. [257] further showed that the rate of HONO production scales linearly with increasing humic acid content in the ice and that extrapolations of the rate meet rates previously found for pure humic acid films and in aqueous aerosol particles. From this they concluded that the general chemistry in ice and in water is identical. Interestingly, this correlation was found to be valid only for small concentrations of humic acid in ice; at higher concentrations the rate of HONO production stagnated. It was concluded that at high concentrations part of the organic material in the ice matrix is no longer accessible to the gaseous NO_2 due to specific agglomeration or displacements in the ice matrix.

Another example of an environmentally relevant species that is strongly involved in redox-cycling is mercury. Mercury is a globally distributed pollutant, and as such is also found in snow and sea ice. Input to the surface snow comes preliminarily from atmospheric deposition [253, 285]. Ocean currents transport most mercury found in sea ice [286]. What makes mercury especially interesting from a chemical point of view is that its environmental fate is largely given by its oxidation state [253, 285]. Elemental mercury, Hg(0), is highly volatile and has a negligible affinity to surfaces such as snow or ice [287]. Divalent mercury, Hg(II), is highly water-soluble and the main oxidation state present in snow and ice. The precise balance between Hg(0) in the gas phase and Hg(II) in the surface snow is not static. For example, during spring episodes so-called Mercury Depletion Events (MDE) occur where Hg(0) is almost completely removed from the air. These events are driven through gas phase chemistry, which converts Hg(0) to Hg(II) that subsequently becomes bound to particles and/or ground snow. Halogen emissions from surface snow are currently thought to trigger those gas phase chemical cycles. Snow may thus act as a reservoir in which mercury is accumulated during winter. In spring this sequestered mercury may be released to the aquatic environment during snowmelt [288] from which it may enter the food chain [289]. Field studies have, however, shown that the Hg(II) initially trapped in the surface snow can be reemitted as Hg(0) to the atmosphere and that this emission is enhanced by solar radiation [290]. This light-driven emission of mercury from the snow thus lowers the overall net transfer of atmospheric mercury to the aquatic environment. Only the fraction of mercury that is buried in the snow below the photolytic zone is inert to photochemistry and can be permanently stored.

The detailed mechanisms and rates of the underlying redox chemistry in ice and snow are still open. In a recent laboratory study, Bartels-Rausch et al. [291] could show that the light-driven emission of Hg(0) from an ice matrix is significantly enhanced in the presence of organic chromophores (Fig. 16). That the photolytic reduction of mercury is enhanced in the presence of organics is well established for the aqueous phase [292]. There, two mechanisms seem to operate simultaneously [293]. Organics easily form complexes with mercuric ions and light absorption of

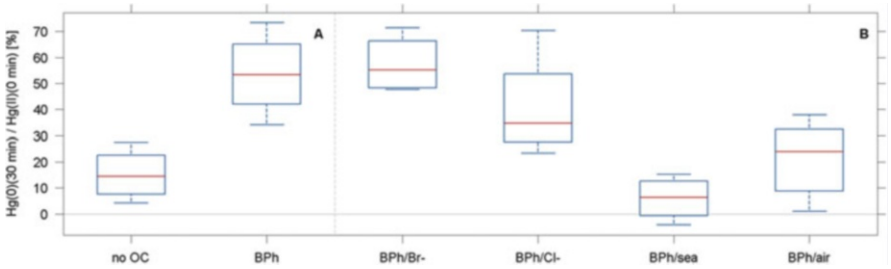

Fig. 16 The effect of organic chromophores, halogens, and oxygen on the light-driven release of elemental mercury from ice films. Results are given relative to the initial concentration of mercuric ions in the ice after 30 min irradiation at 258 K. The solution to freeze the ice films was always doped with Hg(II) (6×10^{-8} M) and additionally contained the following compounds as indicated: "no OC" denotes experiments of pure HgO solutions; "BPh" 6×10^{-7} M benzophenone in unbuffered solutions at pH 7 (of the molten ice film); "BPh/Br^-" 6×10^{-7} M benzophenone and 5×10^{-8} M bromide; "BPh/Cl^-" 7×10^{-8} M chloride; "BPh/sea" 0.5 M chloride, 1 mM bromide; "BPh/air" 6×10^{-7} M benzophenone in the ice – 20% oxygen was present in the carrier gas stream. In each box, the central mark is the median, the edges of the boxes are the 25th and 75th percentiles, and the whiskers extend to the most extreme data points [291]

these complexes can lead to intramolecular redox reactions [294]. Also, the organics can adsorb light and transfer electrons, or energy, intermolecularly, similar to the chemistry described above for nitrogen oxides. In either case, Bartels-Rausch et al. [291] argued that the reduction of Hg(II) to Hg(0) in ice most likely proceeds via Hg(I) as intermediate. They observed that the presence of chloride and of oxygen significantly lowers the photoreactivity of the mercury-organics mixtures in ice, whereas the presence of bromide had little influence. This observation is in line with the oxidation capacity of oxygen and of the halogens in irradiated aqueous solutions [292, 295]. This preservation of mercury in the snow might partially explain the higher mercury concentrations in halogen-rich snow on sea ice as compared to more off-shore samples [253].

Turning our attention to inorganic chromophores, one of the most relevant is certainly H_2O_2. H_2O_2 is ubiquitously present in environmental snow and ice and is an important photolytic OH source [179]. While estimates based on photochemistry in solution indicate a relatively short photolytic lifetime [195], Beine and Anastasio [254] suggest that when H_2O_2 is dissolved in crystalline ice the apparent lifetime becomes significantly longer because cage recombination may occur, while when adsorbed in a QLL or dissolved in a brine, OH may escape as in solution. This is therefore an example where a trace gas may become a solute in crystalline ice, leading to an extended photolytic lifetime.

Of similar photochemical importance as H_2O_2 is nitrate, which absorbs light above 290 nm. The ubiquitous presence of nitrate in environmental ices is well documented for cirrus ice particles [296, 297] as well as permanent and perennial snow packs [298–301]. In aqueous solution, photolysis of nitrate ion leads to either OH and NO_2 or $O(^3P)$ and nitrite ion, with typically significantly higher quantum yields for the first pathway [197, 200]. In the upper troposphere, it is currently thought that uptake of HNO_3 to ice makes it ineffective as a photolytic source of

NO_X as it is in the gas phase, in spite of the fact that the nature of nitrate at the ice surface is not well established. Recent spectroscopic experiments indicate that nitrate exists at the ice surface in solvated form with a local environment similar to that in concentrated solution [302]. Still, this does not rule out a reduced solvent cage compared to dilute nitrate solution that would allow NO_2 to escape, more likely due to recombination being suppressed, as has been suggested based on quantum yield measurements for frozen nitrate solutions [192]. Since in snow the nitrate anion is often co-located with other ions, e.g., halogenide ions, in a brine solution, ion specific effects may lead to enhancement of nitrate ions at the aqueous brine-air interface. Such effects have been shown to lead to enhanced nitrate photolysis rates in aqueous solution [303, 304]. In some contrast to the case of H_2O_2, the particular environment in snow or ice makes photolysis of nitrate more efficient than in solution. Such effects would help to explain the significant cycling of NO_X mediated by nitrate photolysis in polar snow [276, 298, 305–308].

Halogens have not been discussed so far. Halogens are important atmospheric players in stratospheric and tropospheric ozone depletion. In the stratosphere direct photolysis leads to ozone depletion. In surface ice, snow halogens can be activated and released to overlying air, where they foster ozone depletion. In snow or ice the most prevalent condensed phase halogen compounds do not absorb the available light of the solar spectrum. Potentially, interhalogen complexes such as Br_2I^- and BrI_2^- might absorb in the visible wavelengths [309] yet their existence at the low halogen concentrations in typical snow samples is questionable. It might be proposed that the light-induced reaction with excited organic chromophores might be of higher relevance, similar to the chemistry observed in aqueous solutions [295]. This chemistry can interfere with light-driven redox reactions, as discussed above for mercury where halogens can foster the back-reaction of the photochemistry. Additionally, halogens might form complexes with metallic ions such as mercury. Those complexes typically absorb at longer wavelength than the isolated species; mercury-iodine complexes for example absorb at wavelengths above 300 nm [310]. Indirect photochemical processes involving halogen compounds associated with ice have the potential to release Br_2, BrCl or halogenated VOCs that are in turn strongly implicated in gas phase photochemical cycles of the air mass in contact with ice or snow.

In summary, atmospherically relevant photochemistry with environmental ices is initiated by a range of organic and inorganic chromophores. In a wealth of secondary energy transfer and redox processes species of atmospheric relevance may be reduced or oxidized. Recent developments in the field have indicated the role of the specific arrangement of chromophores and reaction partners as well as their molecular level local environment in ice cloud particles, sea ice, or snow packs that will require further attention in the future. Photochemical processes in ice continue to be an important issue in the cycling of major and trace constituents as highlighted in this chapter. They are also linked to albedo changes of the frozen parts of the Earth's surface and thus to the radiative budget of the atmosphere [311]. Furthermore, photochemical processes are important ingredients in the way trace constituents are incorporated into ice archives from which past climates are reconstructed [308].

6 Photochemical processes on natural and built ground surfaces

In the preceding sections we addressed long-wavelength photoassisted reactions as overtone processes and heterogeneous reactions on aerosols (photosensitized and photocatalyzed) or on ice. However, the condensed material initiating these reactions can also (and maybe even predominately) be found on the continental natural or affected ground surface, such as soil, vegetation covered by plant degradation products, and within films coating urban surfaces (such as roads and buildings).

Of special interest are the films on the ground in densely populated and urban areas, also called 'urban grime', whose chemical composition partly resembles that of urban atmospheric aerosols [312–314] but whose chemistry is still almost unknown. In this section, we first turn our attention to urban grime and soil surfaces.

In the past decade or so, extensive work by Diamond and co-workers [312–317] has shown that exposed outdoor surfaces in urban areas rapidly become coated with a complex mixture of chemical compounds ("urban surface film"), most readily encountered as "window grime." This film grows via accretion from the atmosphere and is removed by rain wash-off, or revolatilization processes, yielding an (estimated) steady-state thickness of several tens to hundreds of nanometers. Chemical analysis of these films has been carried out both in a "broad brush" approach [312, 313], which identified the compound classes present, and by more detailed studies [315–317] that determined the specific compounds within these classes.

Interestingly, organics make up only 5–10 mass % of the films; most of the identified mass is nitrate (~7%), sulfate (~8%), and various metals (18%). The organic fraction contains a wide array of natural and anthropogenic chemicals including carbohydrates and aliphatic and aromatic compounds [313–321]. PAHs account for approximately 20% of the organic mass of "urban grime" [313, 314]. Sources of PAHs are incomplete fossil fuel combustion [322], wood burning [323], and industrial processes [324]. Some of these PAHs are reported to have carcinogenic and mutagenic properties [312, 325, 326]; those bearing five aromatic rings or more are predominantly adsorbed onto particulate matter [1] and therefore their lifetime and fate are strongly influenced by heterogeneous oxidative processes [73, 76, 78, 80, 81, 84, 85, 328–341]. Raja and Valsaraj showed that particle bound naphthalene and phenanthrene degrade much faster than in the gas phase [338].

Inorganic compounds represent the major mass fraction of "urban grime." Metals, sulfates and nitrates have been identified as the main components [314, 342]. Deposited nitrate ions can further undergo direct photolysis affecting the atmosphere through the release of volatile and reactive nitrogen compounds to the gas phase [276, 298, 305–308, 342, 343]. However, as shown above, the heterogeneous loss of gas phase molecules at surfaces containing photoreactive compounds may be significantly enhanced under illumination [344–346]. Soot, pyrene, and humic acids promote the photoenhanced heterogeneous removal of NO_2 producing both NO and HONO [124, 347, 348].

In one study [349] nitric acid was deposited from the gas phase onto films prepared to mimic the organic fraction of urban grime [73]. Using acridine,

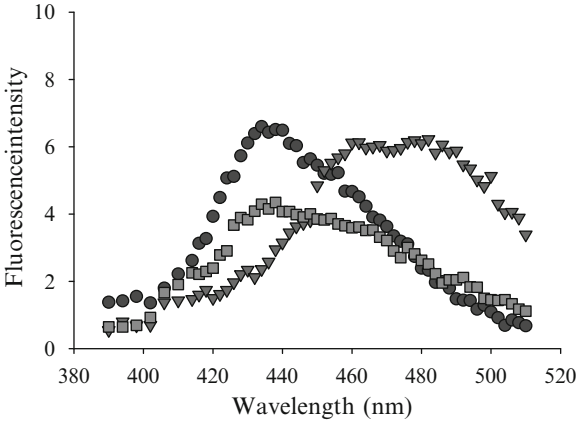

Fig. 17 Fluorescence of acridine in organic film before exposure to gas phase nitric acid (*circles*); following exposure to gas phase acid (*triangles*); and following 90 min of irradiation with actinic light (*squares*)

a pH-sensitive fluorescent probe, acidification of the film upon exposure to HNO_3(g) was observed, indicating that the acid was taken up by the organic film and remained there in (at least partially) dissociated form. Illumination of this acidified film using the output of a Xe lamp, filtered optically to simulate actinic radiation on the Earth's surface, caused the pH to increase, eventually returning to its original value (i.e., that which it displayed before acidification). Figure 17 displays these changes in the emission spectrum. At the same time, the concentration of nitrate anion also diminished, as measured by ion chromatography. Given the known photochemistry of nitrate anion in water and ice [192, 197, 350–352], and other arguments presented in Handley et al. [349], we proposed that these observations indicate that the nitrate anion in organic films could photochemically generate NO_2 and HONO, which are then released to the gas phase.

This could have important atmospheric consequences. Because the primary pathway for removal of inorganic nitrate (nitric acid or ammonium nitrate) from the atmosphere is by wet (i.e., uptake by water droplets) or dry deposition, followed by rainout/wash off to the ground, this photochemical reduction of NO_3^- provides a mechanism to recycle nitrate back to the gas phase as "active" nitrogen oxides (HONO, NO_2, or NO). These observations are finally "similar" to the renoxification processes on dust discussed above.

Ammar et al. [353] studied the heterogeneous reaction between gaseous NO_2 and solid pyrene/KNO_3 films, used as a proxy of "urban grime." The uptake coefficients measured under near-UV irradiation (300–420 nm) were between 7- and 15-fold higher than the uptake under dark conditions, highlighting again a strong photo enhancement (Fig. 18). The gaseous products that were identified were NO and HONO. The HONO yield was as high as 36% depending on the composition of the film.

If extrapolated to the solar spectral irradiance at the Earth's surface under near-UV irradiation, the uptake coefficient (at 50 ppbv of NO_2) becomes $\gamma = (8.8 \pm 0.5) \times 10^{-6}$. Such data can be used to estimate the HONO source flux from these urban surfaces as 130 pptv h^{-1} just by assuming that only 1% of a street-canyon surface with 10 m street width and 20 m building height is covered by

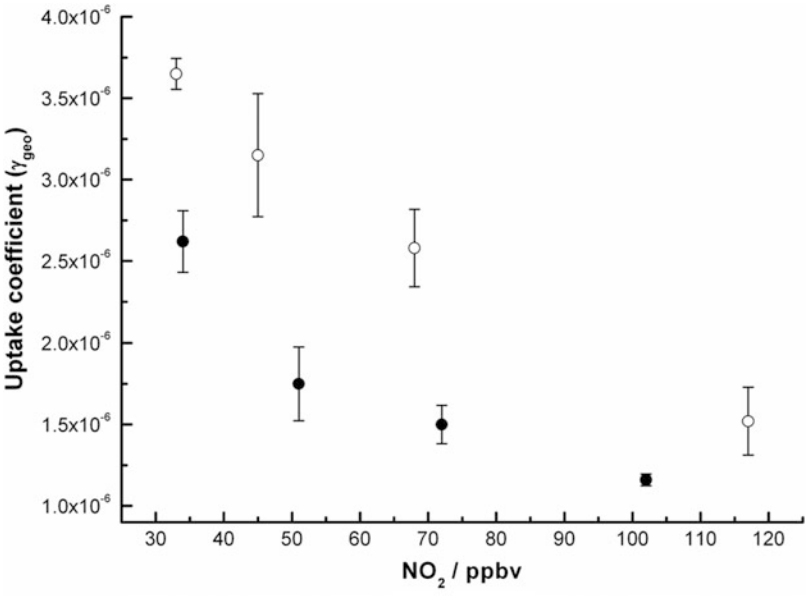

Fig. 18 Steady-state uptake coefficients for the heterogeneous reaction of NO_2 with pyrene films (*empty circles*) and pyrene/nitrate films (*filled circles*) under irradiation as a function of the initial NO_2 concentration. *Errors bar* are 1σ precision

pyrene/nitrate films (it is important to emphasize that this is potentially a quite conservative assumption).

To explain the photoenhanced conversion of NO_2 on pyrene (Py) films into HONO, NO, NO_2^-, and traces of 1-nitropyrene, the following mechanism was suggested:

$$\mathrm{Py} \xrightarrow{h\nu} \mathrm{Py}^* \tag{29}$$

$$\mathrm{Py}^* + \mathrm{NO_2} \rightarrow [\mathrm{Py}^+ + \mathrm{NO_2}^-] \tag{30}$$

$$[\mathrm{Py}^+ + \mathrm{NO_2}^-] \rightarrow \mathrm{Py}' + \mathrm{NO_2}^- \tag{31}$$

$$[\mathrm{Py}^+ + \mathrm{NO_2}^-] \rightarrow \mathrm{PyNO_2} \tag{32}$$

$$\mathrm{NO_2}^- + \mathrm{H}^+ \rightleftarrows \mathrm{HONO} \tag{33}$$

$$\mathrm{NO_2}^- \xrightarrow{h\nu} \mathrm{NO} + \mathrm{O}^- \tag{34}$$

As discussed previously [347, 348], the heterogeneous reaction may proceed via electron transfer from electronically excited states of the PAH (in this specific case pyrene (Py^*)) to NO_2. As indicated in (5), HONO is formed by the acid–base

reaction involving NO_2^-. Miet et al. [337] have suggested HONO formation in the mechanism to explain 1-nitropyrene production. The photo-stability of NO_2^- on the film was tested by Ammar et al. and emission of HONO and NO was indeed observed, implying reactions (5)–(6) [353]. Similar conclusions about the mechanism were also drawn by Sosedova et al. [89], who identified both direct and indirect pathways of HONO formation from exposure of phenolic and polyphenolic compounds to NO_2 and light. HONO was also formed through photolysis of nitrophenols formed as intermediates.

The main conclusion from these observations is that "dirty" urban surfaces may contribute to urban air pollution and promote photochemical pollution.

We finally turn our attention to the natural soil. Soil on Earth is considered to be the layered deposits of parent rock weathering and erosion, which is composed of a large range of organic and mineral components. The relative abundance of these two classes of components varies from pure mineral to almost entirely organic soils. Within the context of atmospheric sciences, soil plays a tremendous role in the biogeochemical cycles of carbon and nitrogen. Soil covers a large fraction of the continental ground surfaces on Earth. Soil is composed of a significant fraction of chromophoric material and is exposed to sunlight for significant periods of time. It is therefore not surprising that the interaction of UV and visible radiation with the biogeochemical cycles has received considerable attention [354]. Such interactions have been investigated mainly in terms of direct and indirect effects of UV radiation on metabolic and abiotic processes that affect carbon sequestration or nutrient cycling. Relatively little attention has been given to direct photochemical processes that would affect deposition to or emission from soil of species implicated in atmospheric chemistry. A few studies have addressed the impact of UV on the net efflux of carbon dioxide and methane [355, 356]. Following up on previous knowledge on the implications of soil processes in the context of the carbon budget, Derendorp et al. [357] specifically determined C2 to C5 hydrocarbon emission rates from irradiated leaf litter. Emission of these saturated and unsaturated hydrocarbons was clearly linked to UV irradiation and the presence of oxygen, providing some evidence for reactive oxygen species inducing lipid peroxidation processes. Degradation of vegetation, and especially lignin, a major structural compound of vegetation, leads to both light absorbing and redox active aromatic compounds as constituents of humic material [358, 359] that are implicated in the production of singlet oxygen, superoxide, or phenoxy type radicals [360]. These in turn are important promoters in the degradation and photobleaching of plant litter itself. However, the radical induced degradation processes also lead to emission of volatile products, such as those observed by Derendorp et al. mentioned above, and also of CO_2 [361] or CO [362, 363]. Some of these emitted species may be directly involved in the photooxidation capacity of the troposphere. This is especially true for the photolytic OH precursors like aldehydes or ketones. Such species have been known to be emitted from degrading plant material [364]. D'Anna et al. [131] observed the emission of several small aldehydes and ketones from humic acid as a result of direct and indirect (sensitized) photochemical processes in the UV and visible wavelengths. The implication to atmospheric chemistry is twofold: these

OVOC species contribute to the atmospheric OH budget. On the other hand, D'Anna et al. also observed a strongly enhanced reaction of humic and fulvic acids with O_3 and suggested that this may be a non-negligible contribution to the overall O_3 deposition to soil. A similar interaction has been discovered by Stemmler et al. [128]. They observed that soil dust or macroscopic soil layers emit nitrous acid (HONO) when exposed to nitrogen dioxide and light (both UV and visible) that showed similar behavior to that observed in similar experiments with humic acids. They suggested that the reaction is due to photosensitized electron transfer from the donating humic acid moieties to nitrogen dioxide. Such a process was suggested before based on similar experiments with mixtures of aromatic ketones and phenolic species [127], which are considered building blocks of humic matter. A third example is the mercury cycle in which photoreduction or photooxidation of Hg(II) and Hg(0), respectively, through radiation induced redox activity of humic material [365, 366], may play an important role in the bioavailability of this toxic compound.

7 Summary and Outlook

The topics discussed in this chapter demonstrate the existence of a wide range of photo-assisted processes in the troposphere not considered in atmospheric models to date. These processes occur through various mechanisms on a wide range of surfaces (including aerosols, urban grime, soil, liquid water, and ice), in aqueous bulk solutions, and in the gas phase (through long wavelength overtone processes).

These sunlight driven processes have only recently been recognized as addressing emerging issues in atmospheric chemistry and so there are still significant gaps in our knowledge limiting our ability to quantify and predict their atmospheric importance. Radical generation may occur in the bulk phase of aqueous particles and thus change reactive radical budgets. However, an important emerging issue is the production of radicals at interfaces; this process may significantly change our understanding of tropospheric heterogeneous chemistry because radicals being formed in such interfacial processes can either increase the gross reactivity of the surface or desorb and become active in the gas phase. Experiments to quantify this radical production under a wider range of chemical composition and conditions are now needed. Excitation of vibrational overtone transitions by red light, followed by molecular dissociation, represents another example of "non-classical" atmospheric photochemistry which may exert a significant influence on radical budgets.

Optical properties of aerosols are currently the focus of many studies aiming to characterize their potential impact on the Earth's albedo and therefore on climate change. However, light-absorbing chemical constituents of aerosols may also change the physico-chemical properties of the particles. The current conceptual view is that trace gases are taken up by aerosols depending on their volatility, the latter being altered by gas phase oxidation processes. If light-absorbing species

present within (or at the surface of) aerosols also act as photosensitizers (which is still an open question), then maybe one should consider the aerosols as being surrounded by reactive oxidizing species or radicals that will certainly alter the phase partitioning of impinging trace gases. If true, this implies that surface reactions are a general phenomenon during daytime in the atmosphere. Additionally, the bulk of particles is probably also chemically very active because of conventional radical chemistry together with species resulting from "new photochemistry." How important may the overall photo-induced chemistry be in terms of coupling air pollution and climate change?

The general sense behind the illustrative examples presented here is that photo-assisted processes are potentially accelerating reactions that would otherwise be too slow to be of any importance, as shown in the case of NO_2 and some organics reacting on dust. But how general is that statement? Do we need to revisit dust chemistry in the upper troposphere? Does this chemistry have the potential to affect the budget of long lived species?

The forecasted impact of climate change is huge and naturally attracts attention. However, air pollution is still an acute issue in the ever growing urban environment, where little attention has been given to the built environment in terms of sinks of pollutants. Given that the surface area of the built environment is by far larger than that exposed by aerosols, we may ask the question whether such surfaces and the urban grime found upon them may be key players in air pollution that have previously been ignored.

Clearly, enhanced radical production through the range of photochemical mechanisms discussed in this chapter could have a significant impact on atmospheric chemistry. Assessing the full extent by which they influence the atmosphere will certainly require further research. We look forward to a new era of atmospheric photochemistry; one which recognizes that the full solar spectrum should be considered as important to the chemistry which affects us all.

References

1. Finlayson-Pitts BJ, Pitts JN (2000) Chemistry of the upper and lower atmosphere: theory, experiments, and applications. Academic, San Diego
2. Calvert JG, Pitts JN (1966) Photochemistry. Wiley, New York
3. Braun AM, Maurette M-Trs, Oliveros E (1986) Technologie photochimique. Presses Polytechniques Romandes
4. Herrmann JM (1999) Catal Today 53:115
5. Hoffmann MR, Martin ST, Choi W, Bahnemann DW (1995) Chem Rev 95:69
6. Lane JR, Kjaergaard HG (2010) J Chem Phys 132. doi:174304 10.1063/1.3408192
7. Donaldson DJ, Orlando JJ, Amann S, Tyndall GS, Proos RJ, Henry BR, Vaida V (1998) J Phys Chem A 102:5171. doi:10.1021/jp980811d
8. Havey DK, Vaida V (2004) J Mol Spectrosc 228:152. doi:10.1016/j.jms.2004.07.015
9. Phillips JA, Orlando JJ, Tyndall GS, Vaida V (1998) Chem Phys Lett 296:377. doi:10.1016/s0009-2614(98)01045-8

10. Plath KL, Axson JL, Nelson GC, Takahashi K, Skodje RT, Vaida V (2009) React Kinet Catal Lett 96:209. doi:10.1007/s11144-009-5528-2
11. Henry BR (1977) Acc Chem Res 10:207
12. Crim FF (1984) Annu Rev Phys Chem 35:657
13. Donaldson DJ, George C, Vaida V (2010) Environ Sci Technol 44:5321. doi:10.1021/es903680v
14. Donaldson DJ, Tuck AF, Vaida V (2003) Chem Rev 103:4717. doi:10.1021/cr0206519
15. Vaida V (2009) J Phys Chem A 113:5. doi:10.1021/jp806365r
16. Vaida V, Feierabend KJ, Rontu N, Takahashi K (2008) Int J Photoenergy. doi:138091 10.1155/2008/138091
17. Matthews J, Fry JL, Roehl CM (2008) J Chem Phys 128: Article 184306
18. Rizzo TR, Hayden CC, Crim FF (1984) J Chem Phys 81:4501. doi:10.1063/1.447419
19. Sinha A, Vanderwal RL, Crim FF (1990) J Chem Phys 92:401. doi:10.1063/1.458442
20. Homitsky SC, Dragulin SM, Haynes LM, Hsieh S (2004) J Phys Chem A 108:9492. doi:10.1021/jp0474551
21. Matthews J, Sinha A (2005) J Chem Phys 122. doi:104313 10.1063/1.1858437
22. Miller Y, Chaban GM, Finlayson-Pitts BJ, Gerber RB (2006) J Phys Chem A 110:5342
23. Zhang H, Roehl CM, Sander SP (2000) J Geophys Res Atmos 105:14593
24. Brown SS, Wilson RW, Ravishankara AR (2000) J Phys Chem A 104:4976. doi:10.1021/jp000439d
25. Stark H, Brown SS, Burkholder JB, Aldener M, Riffault V, Gierczak T, Ravishankara AR (2008) J Phys Chem A 112:9296
26. Donaldson DJ, Frost GJ, Rosenlof KH, Tuck AF, Vaida V (1997) Geophys Res Lett 24:2651. doi:10.1029/97gl02663
27. Donaldson DJ, Tuck AF, Vaida V (2000) Phys Chem Earth Part C 25:223. doi:10.1016/s1464-1917(00)00009-x
28. Murphy JG, Thornton JA, Wooldridge PJ, Day DA, Rosen RS, Cantrell C, Shetter RE, Lefer B, Cohen RC (2004) Atmos Chem Phys 4:377
29. Salawitch RJ, Wennberg PO, Toon GC (2002) Geophys Res Lett 29: Article 1762
30. Wennberg PO, Salawitch RJ, Donaldson DJ, Hanisco TF, Lanzendorf EJ, Perkins KK, Lloyd SA, Vaida V, Gao RS, Hintsa EJ, Cohen RC, Swartz WH, Kusterer TL, Anderson DE (1999) Geophys Res Lett 26:1373. doi:10.1029/1999gl900255
31. Hall GA (1949) J Am Chem Soc 71:2691. doi:10.1021/ja01176a027
32. Staikova M, Oh M, Donaldson DJ (2005) J Phys Chem A 109:597. doi:10.1021/jp046141v
33. Vaida V, Kjaergaard HG, Hintze PE, Donaldson DJ (2003) Science 299:1566
34. Brutti S, Bencivenni L, Barbarossa V, Sau S, De Maria G (2006) J Chem Thermodyn 38:1292. doi:10.1016/j.jct.2006.02.009
35. Mills MJ, Toon OB, Solomon S (1999) Geophys Res Lett 26:1133. doi:10.1029/1999gl900187
36. Lane JR, Kjaergaard HG (2008) J Phys Chem A 112:4958. doi:10.1021/jp710863r
37. Hintze PE, Kjaergaard HG, Vaida V, Burkholder JB (2003) J Phys Chem A 107:1112. doi:10.1021/jp0263626
38. Kjaergaard HG, Lane JR, Garden AL, Schofield DP, Robinson TW, Mills MJ, (2008) Atmospheric photolysis of sulphuric acid. In: Goodsite, Michael E, Johnson, Matthew S (Eds.), Advances in Quantum Chemistry: Applications of Theoretical Methods to Atmospheric Science, Vol. 55. Elsevier, pp. 137–158. Chapter 8.
39. Mills MJ, Toon OB, Thomas GE (2005) J Geophys Res 110:D24208
40. Mills MJ, Toon OB, Vaida V, Hintze PH, Kjaergaard HG, Schofield DP, Robinson TW (2005) J Geophys Res Atmos 110:D08201
41. Hecobian A, Zhang X, Zheng M, Frank N, Edgerton ES, Weber RJ (2010) Atmos Chem Phys 10:5965. doi:10.5194/acp-10-5965-2010
42. Feierabend KJ, Havey DK, Brown SS, Vaida V (2006) Chem Phys Lett 420:438. doi:10.1016/j.cplett.01.013
43. Miller Y, Chaban GM, Gerber RB (2005) J Phys Chem A 109:6565. doi:10.1021/jp058110l
44. Yosa J, Meuwly M (2011) J Phys Chem A 115:14350

45. Miller Y, Gerber RB (2006) J Am Chem Soc 128:9594. doi:Ja062890 10.1021/ja062890+
46. Miller Y, Gerber RB, Vaida V (2007) Geophys Res Lett 34. doi:L16820 10.1029/2007gl030529
47. Zhang X, Liang MC, Montmessin F, Bertaux JL, Parkinson C, Yung YL (2010) Nat Geosci 3:834. doi:10.1038/ngeo989
48. Dunn ME, Shields GC, Takahashi K, Skodje RT, Vaida V (2008) J Phys Chem A 112:10226. doi:10.1021/jp805746t
49. Takahashi K, Plath KL, Axson JL, Nelson GC, Skodje RT, Vaida V (2010) J Phys Chem A 132. doi:10.1021/094305
50. Takahashi K, Plath KL, Skodje RT, Vaida V (2008) J Phys Chem A 112:7321. doi:10.1021/jp803225c
51. Skodje RT (1991) J Chem Phys 95:7234. doi:10.1063/1.461401
52. Kanakidou M, Seinfeld JH, Pandis SN, Barnes I, Dentener FJ, Facchini MC, Van Dingenen R, Ervens B, Nenes A, Nielsen CJ, Swietlicki E, Putaud JP, Balkanski Y, Fuzzi S, Horth J, Moortgat GK, Winterhalter R, Myhre CEL, Tsigaridis K, Vignati E, Stephanou EG, Wilson J (2005) Atmos Chem Phys 5:1053
53. Murphy DM, Cziczo DJ, Froyd KD, Hudson PK, Matthew BM, Middlebrook AM, Peltier RE, Sullivan A, Thomson DS, Weber RJ (2006) J Geophys Res Atmos 111:15. doi:D23s32 10.1029/2006jd007340
54. Zhang Q, Jimenez JL, Canagaratna MR, Allan JD, Coe H, Ulbrich I, Alfarra MR, Takami A, Middlebrook AM, Sun YL, Dzepina K, Dunlea E, Docherty K, DeCarlo PF, Salcedo D, Onasch T, Jayne JT, Miyoshi T, Shimono A, Hatakeyama S, Takegawa N, Kondo Y, Schneider J, Drewnick F, Borrmann S, Weimer S, Demerjian K, Williams P, Bower K, Bahreini R, Cottrell L, Griffin RJ, Rautiainen J, Sun JY, Zhang YM, Worsnop DR (2007) Geophys Res Lett 34:6. doi:L13801 10.1029/2007gl029979
55. Froyd KD, Murphy DM, Sanford TJ, Thomson DS, Wilson JC, Pfister L, Lait L (2009) Atmos Chem Phys 9:4363
56. IPCC (2007) Climate change 2007 - the physical science basis: contribution of working group I to the fourth assessment report of the IPCC. Cambridge University Press, Cambridge, UK
57. IARC (1983) IARC Monogr Eval Carcinog Risk Chem Hum 32:1
58. IARC (1987) IARC Monogr Eval Carcinog Risks Hum Suppl 7:1
59. Donaldson K, Li XY, MacNee W (1998) J Aerosol Sci 29:553
60. Akhter MS, Chughtai AR, Smith DM (1984) J Phys Chem 88:5334
61. Al-Abadleh HA, Grassian VH (2000) J Phys Chem A 104:11926
62. Alcala-Jornod C, van den Bergh H, Rossi MJ (2000) Phys Chem Chem Phys 2:5584
63. Ammann M, Kalberer M, Jost DT, Tobler L, Rossler E, Piguet D, Gäggeler HW, Baltensperger U (1998) Nature 395:157
64. Arens F, Gutzwiller L, Baltensperger U, Gäggeler HW, Ammann M (2001) Environ Sci Technol 35:2191
65. Arens F, Gutzwiller L, Gäggeler HW, Ammann M (2002) Phys Chem Chem Phys 4:3684. doi:10.1039/b201713j
66. Aubin DG, Abbatt JPD (2007) J Phys Chem A 111:6263. doi:10.1021/jp068884h
67. Daly HM, Horn AB (2009) Phys Chem Chem Phys 11:1069. doi:10.1039/b815400g
68. Esteve W, Budzinski H, Villenave E (2004) Atmos Environ 38:6063. doi:10.1016/j.atmosenv.2004.05.059
69. Esteve W, Budzinski H, Villenave E (2006) Atmos Environ 40:201
70. Fan ZH, Kamens RM, Zhang JB, Hu JX (1996) Environ Sci Technol 30:2821
71. Gerecke A, Thielmann A, Gutzwiller L, Rossi MJ (1998) Geophys Res Lett 25:2453
72. Gross S, Bertram AK (2008) J Phys Chem A 112:3104
73. Kahan TF, Kwamena NOA, Donaldson DJ (2006) Atmos Environ 40:3448
74. Kalberer M, Ammann M, Arens F, Gäggeler HW, Baltensperger U (1999) J Geophys Res Atmos 104:13825
75. Karagulian F, Rossi MJ (2007) J Phys Chem A 111:1914. doi:10.1021/jp0670891

76. Kwamena NOA, Clarke JP, Kahan TF, Diamond ML, Donaldson DJ (2007) Atmos Environ 41:37. doi:10.1016/j.atmosenv.2006.08.016
77. Kwamena N-OA, Thornton JA, Abbatt JPD (2004) J Phys Chem A 108:11626
78. Mak J, Gross S, Bertram AK (2007) Geophys Res Lett 34. doi:L10804 10.1029/2006gl029756
79. Mmereki BT, Chaudhuri SR, Donaldson DJ (2003) J Phys Chem A 107:2264
80. Mmereki BT, Donaldson DJ, Gilman JB, Eliason TL, Vaida V (2004) Atmos Environ 38:6091
81. Perraudin E, Budzinski H, Villenave E (2005) Atmos Environ 39:6557. doi:10.1016/j.atmosenv.2005.07.037
82. Perraudin E, Budzinskia H, Villenave E (2007) J Atmos Chem 56:57
83. Pltts JN, Sweetman JA, Zlellnska B, Atklnson R, Wlner AM, Harger WP (1985) Environ Sci Technol 19:1115
84. Pöschl U, Letzel T, Schauer C, Niessner R (2001) J Phys Chem A 105:4029
85. Prince AP, Wade JL, Grassian VH, Kleiber PD, Young MA (2002) Atmos Environ 36:5729
86. Stadler D, Rossi MJ (2000) Phys Chem Chem Phys 2:5420
87. Wang HM, Hasegawa K, Kagaya S (2000) Chemosphere 41:1479
88. Arens F, Gutzwiller L, Gäggeler HW, Ammann M (2002) Phys Chem Chem Phys 4:3684
89. Sosedova Y, Rouviere A, Bartels-Rausch T, Ammann M (2011) Photochem Photobiol Sci 10:1680. doi:10.1039/c1pp 05113j
90. Sosedova Y, Rouviere A, Gäggeler HW, Ammann M (2009) J Phys Chem A 113:10979. doi:10.1021/jp9050462
91. Kirchstetter TW, Novakov T, Hobbs PV (2004) J Geophys Res Atmos 109. doi:D21208 10.1029/2004jd004999
92. Bones DL, Henricksen DK, Mang SA, Gonsior M, Bateman AP, Nguyen TB, Cooper WJ, Nizkorodov SA (2010) J Geophys Res Atmos 115:14. doi:D05203 10.1029/2009jd012864
93. Cappa CD, Che DL, Kessler SH, Kroll JH, Wilson KR (2011) J Geophys Res Atmos 116:12. doi:D15204 10.1029/2011jd015918
94. Martins JV, Artaxo P, Kaufman YJ, Castanho AD, Remer LA (2009) Geophys Res Lett 36. doi:L13810 10.1029/2009gl037435
95. Park K, Chow JC, Watson JG, Trimble DL, Doraiswamy P, Arnott WP, Stroud KR, Bowers K, Bode R, Petzold A, Hansen ADA (2006) J Air Waste Manag Assoc 56:474
96. Alexander DTL, Crozier PA, Anderson JR (2008) Science (Washington, DC) 21:833. doi:10.1126/science.1155296
97. Barnard JC, Volkamer R, Kassianov EI (2008) Atmos Chem Phys 8:6665
98. Chen Y, Bond TC (2010) Atmos Chem Phys 10:1773
99. Russell PB, Bergstrom RW, Shinozuka Y, Clarke AD, DeCarlo PF, Jimenez JL, Livingston JM, Redemann J, Dubovik O, Strawa A (2010) Atmos Chem Phys 10:1155
100. Soto-Garcia LL, Andreae MO, Andreae TW, Artaxo P, Maenhaut W, Kirchstetter T, Novakov T, Chow JC, Mayol-Bracero OL (2011) Atmos Chem Phys 11:4425. doi:10.5194/acp-11-4425-2011
101. Sun HL, Biedermann L, Bond TC (2007) Geophys Res Lett 34:5. doi:L17813 10.1029/2007gl029797
102. Zhang XL, Lin YH, Surratt JD, Zotter P, Prevot ASH, Weber RJ (2011) Geophys Res Lett 38:4. doi:L21810 10.1029/2011gl049385
103. Decesari S, Facchini MC, Matta E, Mircea M, Fuzzi S, Chughtai AR, Smith DM (2002) Atmos Environ 36:1827
104. Gonzalez-Perez JA, Gonzalez-Vila FJ, Almendros G, Knicker H (2004) Environ Int 30:855
105. Hoffer A, Kiss G, Blazso M, Gelencser A (2004) Geophys Res Lett 31. doi:L06115 10.1029/2003gl018962
106. Holmes BJ, Petrucci GA (2006) Environ Sci Technol 40:4983
107. Mayol-Bracero OL, Guyon P, Graham B, Roberts G, Andreae MO, Decesari S, Facchini MC, Fuzzi S, Artaxo P (2002) J Geophys Res Atmos 107:LBA59/1
108. Chang JL, Thompson JE (2009) Atmos Environ 44:541. doi:10.1016/j.atmosenv.2009.10.042

109. Galloway MM, Chhabra PS, Chan AWH, Surratt JD, Flagan RC, Seinfeld JH, Keutsch FN (2009) Atmos Chem Phys 9:3331
110. Gelencser A, Hoffer A, Kiss G, Tombacz E, Kurdi R, Bencze L (2003) J Atmos Chem 45:25. doi:10.1023/a:1024060428172
111. Nguyen TB, Lee PB, Updyke KM, Bones DL, Laskin J, Laskin A, Nizkorodov SA (2012) J Geophys Res Atmos 117. doi:10.1029/2011JD016944
112. Noziere B, Dziedzic P, Cordova A (2007) Geophys Res Lett 34:5. doi:L21812 10.1029/2007gl031300
113. Nozière B, Esteve W (2005) Geophys Res Lett 32. doi:L03812 10.1029/2004gl021942
114. Rincon AG, Guzman MI, Hoffmann MR, Colussi AJ (2009) J Phys Chem A 113:10512. doi:10.1021/jp904644n
115. Canonica S, Hellrung B, Wirz J (2000) J Phys Chem A 104:1226
116. Canonica S, Kohn T, Mac M, Real FJ, Wirz J, Von Gunten U (2005) Environ Sci Technol 39:9182
117. Giese B, Napp M, Jacques O, Boudebous H, Taylor AM, Wirz J (2005) Angew Chem Int Ed 44:4073
118. Baduel C, Voisin D, Jaffrezo JL (2010) Atmos Chem Phys 10:4085. doi:10.5194/acp-10-4085-2010
119. Bateman AP, Nizkorodov SA, Laskin J, Laskin A (2011) Phys Chem Chem Phys 13:12199. doi:10.1039/c1cp20526a
120. Net S, Nieto-Gligorovski L, Gligorovski S, Temime-Rousell B, Barbati S, Lazarou YG, Wortham H (2009) Atmos Environ 43:1683
121. Yu Y, Ezell MJ, Zelenyuk A, Imre D, Alexander L, Ortega J, Thomas JL, Gogna K, Tobias DJ, D'Anna B, Harmon CW, Johnson SN, Finlayson-Pitts BJ (2008) Phys Chem Chem Phys 10:3063. doi:10.1039/b719495a
122. Rincon AG, Guzman MI, Hoffmann MR, Colussi AJ (2010) J Phys Chem Lett 1:368. doi:10.1021/jz900186e
123. Shapiro EL, Szprengiel J, Sareen N, Jen CN, Giordano MR, McNeill VF (2009) Atmos Chem Phys 9:2289
124. Stemmler K, Ndour M, Elshorbany Y, Kleffmann J, D'Anna B, George C, Bohn B, Ammann M (2007) Atmos Chem Phys 7:4237
125. Ammann M, Rössler E, Strekowski R, George C (2005) Phys Chem Chem Phys 7:2513
126. Ndour M, D'Anna B, George C, Ka O, Balkanski Y, Kleffmann J, Stemmler K, Ammann M (2008) Geophys Res Lett 35:5. doi:L05812 10.1029/2007gl032006
127. George C, Strekowski RS, Kleffmann J, Stemmler K, Ammann M (2005) Faraday Discuss 130:195. doi:10.1039/b417888m
128. Stemmler K, Ammann M, Donders C, Kleffmann J, George C (2006) Nature 440:195. doi:10.1038/nature04603
129. Monge ME, D'Anna B, Mazri L, Giroir-Fendler A, Ammann M, Donaldson DJ, George C (2010) Proc Natl Acad Sci. doi:10.1073/pnas.0908341107
130. Aymoz G, Jaffrezo JL, Jacob V, Colomb A, George C (2004) Atmos Chem Phys 4:2499
131. D'Anna B, Jammoul A, George C, Stemmler K, Fahrni S, Ammann M, Wisthaler A (2009) J Geophys Res Atmos 114. doi:D12301 10.1029/2008jd011237
132. Staehelin J, Hoigne J (1983) Vom Wasser 61:337
133. Graber ER, Rudich Y (2006) Atmos Chem Phys 6:729
134. Baduel C, Monge ME, Voisin D, Jaffrezo JL, George C, El Haddad I, Marchand N, D'Anna B (2011) Environ Sci Technol 45:5238. doi:10.1021/es200587z
135. Miao HF, Tao WY (2008) J Chem Technol Biotechnol 83:336. doi:10.1002/jctb.1816
136. Allard B, Boren H, Pettersson C, Zhang G (1994) Environ Int 20:97. doi:10.1016/0160-4120(94)90072-8
137. Corin N, Backlund P, Kulovaara M (1996) Chemosphere 33:245. doi:10.1016/0045-6535(96)00167-1
138. Dahlen J, Bertilsson S, Pettersson C (1996) Environ Int 22:501. doi:10.1016/0160-4120(96)00038-4

139. Zelenay V, Monge ME, D'Anna B, George C, Styler SA, Huthwelker T, Ammann M (2011) J Geophys Res 116. doi:D11301 10.1029/2010jd015500
140. Rouvière A, DeCarlo PF, Schlierf A, Favez O, D'Anna B, George C, Prévôt A, Ammann M (2009) Geochim Cosmochim Acta 73:A1125
141. Monge ME, Rosenørn T, Favez O, Müller M, Adler G, Riziq AA, Rudich Y, Herrmann H, George C, D'Anna B (2012) Proc Natl Acad Sci www.pnas.org/cgi/doi/10.1073/pnas.1120593109,109, 6840-6844.
142. Aguer JP, Richard C (1996) J Photochem Photobiol A Chem 93:193
143. Baxter RM, Carey JH (1983) Nature 306:575. doi:10.1038/306575a0
144. Latch DE, McNeill K (2006) Science 311:1743. doi:10.1126/science.1121636
145. Tegen I, Lacis AA (1996) J Geophys Res 101:19237
146. Sassen K, DeMott PJ, Prospero JM, Poellot MR (2003) Geophys Res Lett 30. doi:10.1029/2003gl017371
147. Ansmann A, Mattis I, Muller D, Wandinger U, Radlach M, Althausen D, Damoah R (2005) J Geophys Res Atmos 110. doi:10.1029/2004jd005000
148. Twomey SA, Piepgrass M, Wolfe TL (1984) Tellus Ser B Chem Phys Meteorol 36:356
149. Chang RYW, Sullivan RC, Abbatt JPD (2005) Geophys Res Lett 32:L14815/1
150. Hanisch F, Crowley JN (2003) Phys Chem Chem Phys 5:883
151. Seisel S, Keil T, Lian Y, Zellner R (2006) Int J Chem Kinet 38:242
152. Underwood GM, Li P, Al-Abadleh H, Grassian VH (2001) J Phys Chem A 105:6609
153. Usher CR, Al-Hosney H, Carlos-Cuellar S, Grassian VH (2002) J Geophys Res 107:ACH16/1
154. Vlasenko A, Huthwelker T, Gäggeler HW, Ammann M (2009) Phys Chem Chem Phys 11:7921. doi:10.1039/b904290n
155. Vlasenko A, Sjogren S, Weingartner E, Stemmler K, Gäggeler HW, Ammann M (2006) Atmos Chem Phys 6:2147
156. Falkovich AH, Schkolnik G, Ganor E, Rudich Y (2004) J Geophys Res 109. doi:D02208 10.1029/2003jd003919
157. Sullivan RC, Guazzotti SA, Sodeman DA, Prather KA (2007) Atmos Chem Phys 7:1213
158. Dentener FJ, Carmichael GR, Zhang Y, Lelieveld J, Crutzen PJ (1996) J Geophys Res 101:22869
159. Bauer SE, Balkanski Y, Schulz M, Hauglustaine DA, Dentener F (2004) J Geophys Res 109: D02304/1
160. Phadnis MJ, Carmichael GR (2000) J Atmos Chem 36:285. doi:10.1023/a:1006391626069
161. Song CH, Carmichael GR (2001) J Geophys Res Atmos 106:18131. doi:10.1029/2000jd900352
162. Savoie DL, Prospero JM, Saltzman ES (1989) J Geophys Res 94:5069. doi:10.1029/JD094iD04p05069
163. Baker AR, Kelly SD, Biswas KF, Witt M, Jickells TD (2003) Geophys Res Lett 30. doi:2296 10.1029/2003gl018518
164. Usher CR, Michel AE, Grassian VH (2003) Chem Rev 103:4883
165. Linke C, Moehler O, Veres A, Mohacsi A, Bozoki Z, Szabo G, Schnaiter M (2006) Atmos Chem Phys 6:3315
166. Hanisch F, Crowley JN (2001) J Phys Chem A 105:3096
167. Deguillaume L, Leriche M, Desboeufs K, Mailhot G, George C, Chaumerliac N (2005) Chem Rev 105:3388. doi:10.1021/cr040649c
168. Yumoto H, Matsudo S, Akashi K (2002) Vacuum 65:509
169. Gustafsson RJ, Orlov A, Griffiths PT, Cox RA, Lambert RM (2006) Chem Commun (Cambridge, UK) 3936
170. Langridge JM, Gustafsson RJ, Griffiths PT, Cox RA, Lambert RM, Jones RL (2009) Atmos Environ 43:5128. doi:10.1016/j.atmosenv.2009.06.046
171. Linsebigler AL, Lu GQ, Yates JT (1995) Chem Rev 95:735. doi:10.1021/cr00035a013

172. George C, Ndour M, Balkanski Y, Ka O (2007) In: Mellouki A, Ravishankara AR (eds) Regional climate variability and its impacts in the Mediterranean area. Springer, Dordrecht, p 219
173. Ndour M, Nicolas M, D'Anna B, Ka O, George C (2009) Phys Chem Chem Phys 11:1312. doi:10.1039/b806441e
174. Nicolas M, Ndour M, Ka O, D'Anna B, George C (2009) Environ Sci Technol 43:7437. doi:10.1021/es901569d
175. Sassine M, Burel L, D'Anna B, George C (2010) Atmos Environ 44:5468. doi:10.1016/j.atmosenv.2009.07.044
176. Rubasinghege G, Elzey S, Baltrusaitis J, Jayaweera PM, Grassian VH (2010) J Phys Chem Lett 1:1729. doi:10.1021/jz100371d
177. Ndour M, Conchon P, D'Anna B, Ka O, George C (2009) Geophys Res Lett 36:4. doi:L05816 10.1029/2008gl036662
178. Crowley JN, Ammann M, Cox RA, Hynes RG, Jenkin ME, Mellouki A, Rossi MJ, Troe J, Wallington TJ (2010) Atmos Chem Phys 10:9059. doi:10.5194/acp-10-9059-2010
179. Anastasio C, Galbavy ES, Hutterli MA, Burkhart JF, Friel DK (2007) Atmos Environ 41:5110. doi:10.1016/j.atmosenv.2006.12.011
180. Gustafsson RJ, Orlov A, Griffiths PT, Cox RA, Lambert RM (2006) Chem Commun 3936
181. Beaumont SK, Gustafsson RJ, Lambert RM (2009) Chemphyschem 10:331
182. Dalton JS, Janes PA, Jones NG, Nicholson JA, Hallam KR, Allen GC (2002) Environ Pollut 120:415
183. Usher CR, Grassian VH (2001) Abstracts of papers, 222nd ACS National Meeting, Chicago, IL, United States, August 26–30, 2001: PHYS
184. Ibusuki T, Takeuchi K (1994) J Mol Catal 88:93
185. Lin YM, Tseng YH, Huang JH, Chao CC, Chen CC, Wang I (2006) Environ Sci Technol 40:1616. doi:10.1021/es051007p
186. Ohko Y, Nakamura Y, Fukuda A, Matsuzawa S, Takeuchi K (2008) J Phys Chem C 112:10502. doi:10.1021/jp802959c
187. Chen HH, Navea JG, Young MA, Grassian VH (2011) J Phys Chem A 115:490. doi:10.1021/jp110164j
188. Chen HH, Stanier CO, Young MA, Grassian VH (2011) J Phys Chem A 115:11979. doi:10.1021/jp208164v
189. Meland B, Kleiber PD, Grassian VH, Young MA (2011) J Quant Spectrosc Radiat Transfer 112:1108. doi:10.1016/j.jqsrt.2010.12.002
190. Styler SA, Donaldson DJ (2011) Environ Sci Technol 45:10004. doi:10.1021/es202263q
191. Bones DL, Phillips LF (2009) Phys Chem Chem Phys 11:5392
192. Chu L, Anastasio C (2003) J Phys Chem A 107:9594
193. Fischer M, Warneck P (1996) J Phys Chem 100:18749
194. France JL, King MD, Lee-Taylor J (2007) Atmos Environ 41:5502
195. Goldstein S, Rabani J (2007) J Am Chem Soc 129:10597
196. Vaughan PP, Blough NV (1998) Environ Sci Technol 32:2947
197. Zellner R, Exner M, Herrmann H (1990) J Atmos Chem 10:411
198. Karagulian F, Dilbeck CW, Finlayson-Pitts BJ (2008) J Am Chem Soc 130:11272. doi:10.1021/ja8041965
199. Benkelberg HJ, Warneck P (1995) J Phys Chem 99:5214
200. Herrmann H (2007) Phys Chem Chem Phys 9:3935
201. Herrmann H, Hoffmann D, Schaefer T, Brauer P, Tilgner A (2010) Chemphyschem 11:3796
202. Canonica S, Jans U, Stemmler K, Hoigné J (1995) Environ Sci Technol 29:1822
203. Faust BC, Zepp RG (1993) Environ Sci Technol 27:2517
204. Weller C, Herrmann H (2012) submitted to the "Journal of Photochemistry and Photobiology A: Chemistry"
205. Herrmann H, Tilgner A, Barzaghi P, Majdik Z, Gligorovski S, Poulain L, Monod A (2005) Atmos Environ 39:4351

206. Hatchard CG, Parker CA (1956) Proc R Soc Lond A Math Phys Sci 235:518
207. Cooper GD, Degraff BA (1971) J Phys Chem 75:2897
208. Cooper GD, Degraff BA (1972) J Phys Chem 76:2618
209. Doetschman DC, Dwyer DW, Trojan KL (1989) Chem Phys 129:285
210. Ingram DJE, Hodgson WG, Parker CA, Rees WT (1955) Nature 176:1227
211. Jamieson RA, Perone SP (1972) J Phys Chem 76:830
212. Loginov AV, Katenin SB, Voyakin IV, Shagisultanova GA (1986) Sov J Coord Chem 12:1621
213. Nadtochenko V, Kiwi J (1996) J Photochem Photobiol A Chem 99:145
214. Parker CA (1954) Trans Faraday Soc 50:1213
215. Parker CA, Hatchard CG (1959) J Phys Chem 63:22
216. Patterson JIH, Perone SP (1973) J Phys Chem 77:2437
217. Rehorek D, Benedix M, Thomas P (1977) Inorg Chim Acta 25:L100
218. Rehorek D, Grikos H, Billing R (1990) Z Chem 30:378
219. Pozdnyakov IP, Kel OV, Plyusnin VF, Grivin VP, Bazhin NM (2008) J Phys Chem A 112:8316
220. Mulazzani QG, Dangelantonio M, Venturi M, Hoffman MZ, Rodgers MAJ (1986) J Phys Chem 90:5347
221. Chen J, Zhang H, Tomov IV, Wolfsherg M, Ding XL, Rentzepis PM (2007) J Phys Chem A 111:9326
222. Chen J, Dvornikov AS, Rentzepis PM (2009) J Phys Chem A 113:8818
223. Pozdnyakov IP, Kel OV, Plyusnin VF, Grivin VP, Bazhin NM (2009) J Phys Chem A 113:8820
224. Ciesla P, Kocot P, Mytych P, Stasicka Z (2004) J Mol Catal A Chem 224:17
225. Horváth O, Stevenson KL (1993) Charge transfer photochemistry of coordination compounds. VCH, New York
226. Feng W, Nansheng D, Glebov EM, Pozdnyakov IP, Grivin VP, Plyusnin VF, Bazhin NM (2007) Russ Chem Bull 56:900
227. Glebov EM, Pozdnyakov IP, Grivin VP, Plyusnin VF, Zhang X, Wu F, Deng N (2011) Photochem Photobiol Sci 10:425
228. Plyusnin VF, Pozdnyakov IP, Glebov EM, Grivin VP, Bazhin NM (2009) In: Bahadir AM, Duca G (eds) The role of ecological chemistry in pollution research and sustainable development. Springer, Berlin, p 65
229. Pozdnyakov IP, Glebov EM, Plyusnin VF, Grivin VP, Bunduki E, Goryacheva NV, Gladki V, Duka GG (2009) High Energy Chem (Translation of Khimiya Vysokikh Energii) 43:406
230. Zhang X, Gong Y, Wu F, Deng N, Pozdnyakov IP, Glebov EM, Grivin VP, Plyusnin VF, Bazhin NM (2009) Russ Chem Bull 58:1828
231. Abel B, Assmann J, Buback M, Grimm C, Kling M, Schmatz S, Schroeder J, Witte T (2003) J Phys Chem A 107:9499
232. Bockman TM, Hubig SM, Kochi JK (1997) J Org Chem 62:2210
233. Hilborn JW, Pincock JA (1991) J Am Chem Soc 113:2683
234. von Sonntag C, Schuchmann HP (1991) Angew Chem 30:1255
235. Abrahamson HB, Rezvani AB, Brushmiller JG (1994) Inorg Chim Acta 226:117
236. Voelker BM, Morel FMM, Sulzberger B (1997) Environ Sci Technol 31:1004
237. Kuo DTF, Kirka DW, Jiaa CQ (2006) J Sulfur Chem 27:461
238. Wang L, Zhang CB, Wu F, Deng NS (2006) J Coord Chem 59:803
239. Zuo YG, Hoigne J (1992) Environ Sci Technol 26:1014
240. Zuo YG, Hoigne J (1994) Atmos Environ 28:1231
241. Zuo YG, Zhan J (2005) Atmos Environ 39:27
242. Pehkonen SO, Siefert R, Erel Y, Webb S, Hoffmann MR (1993) Environ Sci Technol 27:2056
243. Franch MI, Ayllon JA, Peral J, Domenech X (2004) Appl Catal B 50:89
244. Duka GG, Batyr DG, Romanchuk LS, Sychev AY (1990) Sov J Coord Chem 16:93
245. Wang Z, Chen X, Ji H, Ma W, Chen C, Zhao J (2010) Environ Sci Technol 44:263

246. Sun LH, Wu CH, Faust BC (1998) J Phys Chem A 102:8664
247. Okochi H, Brimblecombe P (2002) Scientific World 2:767. doi:10.1100/tsw.2002.132
248. Tilgner A, Herrmann H (2010) Atmos Environ 44:5415. doi:10.1016/j.atmosenv.2010.07.050
249. Wolke R, Sehili AM, Simmel M, Knoth O, Tilgner A, Herrmann H (2005) Atmos Environ 39:4375
250. Domine F, Albert M, Huthwelker T, Jacobi HW, Kokhanovsky AA, Lehning M, Picard G, Simpson WR (2008) Atmos Chem Phys 8:171
251. Grannas AM, Jones AE, Dibb J, Ammann M, Anastasio C, Beine HJ, Bergin M, Bottenheim J, Boxe CS, Carver G, Chen G, Crawford JH, Domine F, Frey MM, Guzman MI, Heard DE, Helmig D, Hoffmann MR, Honrath RE, Huey LG, Hutterli M, Jacobi HW, Klan P, Lefer B, McConnell J, Plane J, Sander R, Savarino J, Shepson PB, Simpson WR, Sodeau JR, von Glasow R, Weller R, Wolff EW, Zhu T (2007) Atmos Chem Phys 7:4329
252. Simpson WR, von Glasow R, Riedel K, Anderson P, Ariya P, Bottenheim J, Burrows J, Carpenter LJ, Friess U, Goodsite ME, Heard D, Hutterli M, Jacobi HW, Kaleschke L, Neff B, Plane J, Platt U, Richter A, Roscoe H, Sander R, Shepson P, Sodeau J, Steffen A, Wagner T, Wolff E (2007) Atmos Chem Phys 7:4375
253. Steffen A, Douglas T, Amyot M, Ariya P, Aspmo K, Berg T, Bottenheim J, Brooks S, Cobbett F, Dastoor A, Dommergue A, Ebinghaus R, Ferrari C, Gardfeldt K, Goodsite ME, Lean D, Poulain AJ, Scherz C, Skov H, Sommar J, Temme C (2008) Atmos Chem Phys 8:1445
254. Beine H, Anastasio C (2011) J Geophys Res Atmos 116. doi:D14302 10.1029/2010jd015531
255. Rowland GA, Bausch AR, Grannas AM (2011) Environ Pollut 159:1076. doi:10.1016/j.envpol.2011.02.026
256. Rowland GA, Grannas AM (2011) Cold Reg Sci Technol 66:75. doi:10.1016/j.coldregions.2011.01.009
257. Bartels-Rausch T, Brigante M, Elshorbany YF, Ammann M, D'Anna B, George C, Stemmler K, Ndour M, Kleffmann J (2010) Atmos Environ 44:5443. doi:10.1016/j.atmosenv.2009.12.025
258. Huthwelker T, Ammann M, Peter T (2006) Chem Rev 106:1375
259. Henson BF, Robinson JM (2004) Phys Rev Lett 92. doi:246107 10.1103/PhysRevLett.92.246107
260. Ebert M, Worringen A, Benker N, Mertes S, Weingartner E, Weinbruch S (2011) Atmos Chem Phys 11:2805. doi:10.5194/acp-11-2805-2011
261. Kuo MH, Moussa SG, McNeill VF (2011) Atmos Chem Phys 11:9971
262. Kerbrat M, Pinzer B, Huthwelker T, Gäggeler HW, Ammann M, Schneebeli M (2008) Atmos Chem Phys 8:1261
263. Pinzer BR, Schneebeli M (2009) Geophys Res Lett 36. doi:L23503 10.1029/2009gl039618
264. Schneebeli M, Sokratov SA (2004) Hydrol Processes 18:3655
265. Kaempfer TU, Hopkins MA, Perovich DK (2007) J Geophys Res Atmos 112. doi:D24113 10.1029/2006jd008239
266. Maus S, Muller S, Buttner J, Brütsch S, Huthwelker T, Schwikowski M, Enzmann F, Vahatolo A (2011) Ann Glaciol 52:301
267. Stedmon CA, Thomas DN, Papadimitriou S, Granskog MA, Dieckmann GS (2011) J Geophys Res Biogeosci 116. doi:G0302710.1029/2011jg001716
268. Tepavitcharova S, Todorov T, Rabadjieva D, Dassenakis M, Paraskevopoulou V (2011) Environ Monit Assess 180:217. doi:10.1007/s10661-010-1783-y
269. Wells AJ, Wettlaufer JS, Orszag SA (2011) Geophys Res Lett 38. doi:L04501 10.1029/2010gl046288
270. Obbard RW, Roscoe HK, Wolff EW, Atkinson HM (2009) J Geophys Res 114
271. Beine H, Anastasio C, Esposito G, Patten K, Wilkening E, Domine F, Voisin D, Barret M, Houdier S, Hall S (2011) J Geophys Res 116:D00R05
272. Boxe CS, Saiz-Lopez A (2008) Atmos Chem Phys 8:4855
273. Cho H, Shepson PB, Barrie LA, Cowin JP, Zaveri R (2002) J Phys Chem B 106:11226
274. Wren SN, Donaldson DJ (2011) J Phys Chem Lett 2:1967. doi:10.1021/jz2007484

275. Chu L, Anastasio C (2007) Environ Sci Technol 41:3626. doi:10.1021/es062731q
276. Jacobi HW, Annor T, Quansah E (2006) J Photochem Photobiol A Chem 179:330. doi:10.1016/j.jphotochem.2005.09.001
277. Ram K, Anastasio C (2009) Atmos Environ 43:2252. doi:10.1016/j.atmosenv.2009.01.044
278. Kahan TF, Donaldson DJ (2007) J Phys Chem A 111:1277. doi:10.1021/jp066660t
279. Kahan TF, Donaldson DJ (2010) Environ Sci Technol 44:3819. doi:10.1021/es100448h
280. Wren SN, Donaldson DJ (2010) Phys Chem Chem Phys 12:2648. doi:10.1039/b922254e
281. Kahan TF, Zhao R, Jumaa KB, Donaldson DJ (2010) Environ Sci Technol 44:1302. doi:10.1021/es9031612
282. Ardura D, Kahan TF, Donaldson DJ (2009) J Phys Chem A 113:7353. doi:10.1021/jp811385m
283. Heger D, Nachtigallova D, Surman F, Krausko J, Magyarova B, Brumovsky M, Rubes M, Gladich I, Klan P (2011) J Phys Chem A 115:11412. doi:10.1021/jp205627a
284. Villena G, Wiesen P, Cantrell CA, Flocke F, Fried A, Hall SR, Hornbrook RS, Knapp D, Kosciuch E, Mauldin RL III, McGrath JA, Montzka D, Richter D, Ullmann K, Walega J, Weibring P, Weinheimer A, Staebler RM, Liao J, Huey LG, Kleffmann J (2011) J Geophys Res 116:D00R07
285. Durnford D, Dastoor A (2011) J Geophys Res 116. doi:10.1029/2010JD014809
286. Chaulk A, Stern GA, Armstrong D, Barber DG, Wang F (2011) Environ Sci Technol 45:1866. doi:10.1021/es103434c
287. Bartels-Rausch T, Huthwelker T, Jöri M, Gäggeler HW, Ammann M (2008) Environ Res Lett 045009
288. Mann E, Meyer T, Mitchell CPJ, Wania F (2011) J Environ Monit 13:2695. doi:10.1039/c1em10297d
289. Larose C, Dommergue Al, Marusczak N, Coves J, Ferrari CP, Schneider D (2011) Environ Sci Technol 110222143737064. doi:10.1021/es103016x
290. Lalonde J, Poulain A, Amyot M (2002) Environ Sci Technol 36:174
291. Bartels-Rausch T, Krysztofiak G, Bernhard A, Schläppi M, Schwikowski M, Ammann M (2011) Chemosphere 82:199. doi:10.1016/j.chemosphere.2010.10.020
292. Zhang H (2006) Recent Dev Mercury Sci 37. doi:10.1007/430_015
293. Si L, Ariya PA (2008) Environ Sci Technol 42:5150. doi:10.1021/es800552z
294. Gardfeldt K, Jonsson M (2003) J Phys Chem A 107:4478. doi:10.1021/jp0275342
295. Jammoul A, Dumas S, D'Anna B, George C (2009) Atmos Chem Phys 9:4229
296. Popp PJ, Gao RS, Marcy TP, Fahey DW, Hudson PK, Thompson TL, Karcher B, Ridley BA, Weinheimer AJ, Knapp DJ, Montzka DD, Baumgardner D, Garrett TJ, Weinstock EM, Smith JB, Sayres DS, Pittman JV, Dhaniyala S, Bui TP, Mahoney MJ (2004) J Geophys Res Atmos 109
297. Voigt C, Karcher B, Schlager H, Schiller C, Kramer M, de Reus M, Vossing H, Borrmann S, Mitev V (2007) Atmos Chem Phys 7:3373
298. Frey MM, Savarino J, Morin S, Erbland J, Martins JMF (2009) Atmos Chem Phys 9:8681
299. Helmig D, Seok B, Williams MW, Hueber J, Sanford R Jr (2009) Biogeochemistry 95:115. doi:10.1007/s10533-009-9312-1
300. Hiltbrunner E, Schwikowski M, Korner C (2005) Atmos Environ 39:2249. doi:10.1016/j.atmosenv.2004.12.037
301. Schwikowski M, Brutsch S, Gaggeler HW, Schotterer U (1999) J Geophys Res Atmos 104:13709. doi:10.1029/1998jd100112
302. Krepelova A, Newberg J, Huthwelker T, Bluhm H, Ammann M (2010) Phys Chem Chem Phys 12:8870
303. Richards NK, Wingen LM, Callahan KM, Nishino N, Kleinman MT, Tobias DJ, Finlayson-Pitts BJ (2011) J Phys Chem A 115:5810
304. Wingen LM, Moskun AC, Johnson SN, Thomas JL, Roeselova M, Tobias DJ, Kleinman MT, Finlayson-Pitts BJ (2008) Phys Chem Chem Phys 10:5668
305. Bock J, Jacobi H-W (2011) J Phys Chem A 114:1790. doi:10.1021/jp909205e

306. Jacobi H-W, Hilker B (2007) J Photochem Photobiol A Chem 185:371. doi:10.1016/j.jphotochem.2006.06.039
307. Morin S, Savarino J, Frey MM, Domine F, Jacobi HW, Kaleschke L, Martins JMF (2009) J Geophys Res Atmos 114. doi:D05303 10.1029/2008jd010696
308. Morin S, Savarino J, Frey MM, Yan N, Bekki S, Bottenheim JW, Martins JMF (2008) Science 322:730. doi:10.1126/science.1161910
309. O'Sullivan D, Sodeau JR (2010) J Phys Chem A 114:12208. doi:10.1021/jp104910p
310. Kunkely H, Horvath O, Vogler A (1997) Coord Chem Rev 159:85. doi:10.1016/S0010-8545(96)01307-0
311. France JL, King MD, Lee-Taylor J, Beine HJ, Ianniello A, Domine F, MacArthur A (2011) J Geophys Res Earth Surf 116:16. doi:F04013 10.1029/2011jf002019
312. Hakura A, Shimada H, Nakajima M, Sui H, Kitamoto S, Suzuki S, Satoh T (2005) Mutagenesis 20:217. doi:10.1093/mutage/gei029
313. Simpson AJ, Lam B, Diamond ML, Donaldson DJ, Lefebvre BA, Moser AQ, Williams AJ, Larin NI, Kvasha MP (2006) Chemosphere 63:142
314. Lam B, Diamond ML, Simpson AJ, Makar PA, Truong J, Hernandez-Martinez NA (2005) Atmos Environ 39:6578
315. Butt CM, Diamond ML, Truong J, Ikonomou MG, Helm PA, Stern GA (2004) Environ Sci Technol 38:3514
316. Diamond ML, Gingrich SE, Fertuck K, McCarry BE, Stern GA, Billeck B, Grift B, Brooker D, Yager TD (2000) Environ Sci Technol 34:2900
317. Gingrich SE, Diamond ML (2001) Environ Sci Technol 35:4031
318. Butt CM, Diamond ML, Truong J, Ikonomou MG, Helm PA, Stern GA (2004) Environ Sci Technol 38:3514. doi:10.1021/es0498282
319. Hodge EM, Diamond ML, McCarry BE, Stern GA, Harper PA (2003) Arch Environ Contam Toxicol 44:421. doi:10.1007/s00244-002-1272-6
320. Liu Q-T, Chen R, McCarry BE, Diamond ML, Bahavar B (2003) Environ Sci Technol 37:2340. doi:10.1021/es020848i
321. Liu Q-T, Diamond ML, Gingrich SE, Ondov JM, Maciejczyk P, Stern GA (2003) Environ Pollut 122:51
322. Marr LC, Kirchstetter TW, Harley RA, Miguel AH, Hering SV, Hammond SK (1999) Environ Sci Technol 33:3091. doi:10.1021/es981227l
323. Kleeman MJ, Robert MA, Riddle SG, Fine PM, Hays MD, Schauer JJ, Hannigan MP (2008) Atmos Environ 42:3059
324. Yang H-H, Lee W-J, Chen S-J, Lai S-O (1998) J Hazard Mater 60:159
325. Atkinson R, Arey J (1994) Environ Health Perspect 102:117
326. Durant JL, Lafleur AL, Plummer EF, Taghizadeh K, Busby WF, Thilly WG (1998) Environ Sci Technol 32:1894. doi:10.1021/es9706965
327. Gross S, Bertram AK (2008) J Phys Chem A 112:3104. doi:10.1021/jp7107544
328. Kahan TF, Donaldson DJ (2008) Environ Res Lett 3:6. doi:045006 10.1088/1748-9326/3/4/045006
329. Kong L, Ferry JL (2004) J Photochem Photobiol A 162:415
330. Kwamena NOA, Abbatt JPD (2008) Atmos Environ 42:8309. doi:10.1016/j.atmosenv.2008.07.037
331. Kwamena NOA, Staikova MG, Donaldson DJ, George IJ, Abbatt JPD (2007) J Phys Chem A 111:11050. doi:10.1021/jp075300i
332. Kwamena N-OA, Earp ME, Young CJ, Abbatt JPD (2006) J Phys Chem A 110:3638. doi:10.1021/jp056125d
333. Kwamena N-OA, Thornton JA, Abbatt JPD (2004) J Phys Chem A 108:11626. doi:10.1021/jp046161x
334. McCabe J, Abbatt JPD (2009) J Phys Chem C 113:2120. doi:10.1021/jp806771q
335. Miet K, Le Menach K, Flaud PM, Budzinski H, Villenave E (2009) Atmos Environ 43:837. doi:10.1016/j.atmosenv.2008.10.041

336. Nielsen T (1984) Environ Sci Technol 18:157
337. Pryor WA, Gleicher GJ, Cosgrove JP, Church DF (1984) J Org Chem 49:5189. doi:10.1021/jo00200a035
338. Raja S, Valsaraj KT (2005) J Air Waste Manage Assoc 55:1345
339. Ridd JH (1998) Acta Chem Scand 52:11
340. Zhang Y, Yang B, Meng J, Gao S, Dong X, Shu J (2010) Atmos Environ 44:697
341. Wang XF, Zhang YP, Chen H, Yang X, Chen JM, Geng FH (2009) Environ Sci Technol 43:3061. doi:10.1021/es8020155
342. Honrath RE, Peterson MC, Guo S, Dibb JE, Shepson PB, Campbell B (1999) Geophys Res Lett 26:695
343. Jacobi H-W, Hilker B (2007) J Photochem Photobiol A 185:371
344. Jammoul A, Gligorovski S, George C, D'Anna B (2008) J Phys Chem A 112:1268. doi:10.1021/jp074348t
345. Reeser DI, Jammoul A, Clifford D, Brigante M, D'Anna B, George C, Donaldson DJ (2008) J Phys Chem C 113:2071. doi:10.1021/jp805167d
346. Styler SA, Brigante M, D'Anna B, George C, Donaldson DJ (2009) Phys Chem Chem Phys 11:7876. doi:10.1039/b904180j
347. Brigante M, Cazoir D, D'Anna B, George C, Donaldson DJ (2008) J Phys Chem A 112:9503. doi:10.1021/jp802324g
348. Monge ME, D'Anna B, Mazri L, Giroir-Fendler A, Ammann M, Donaldson DJ, George C (2010) Proc Natl Acad Sci USA 107:6605
349. Handley SR, Clifford D, Donaldson DJ (2007) Environ Sci Technol 41:3898
350. Bartels-Rausch T, Donaldson DJ (2006) Atmos Chem Phys Discuss 6:10713
351. Vione D, Maurino V, Minero C, Pelizzetti E, Harrison MAJ, Olariu RI, Arsene C (2006) Chem Soc Rev 35:441
352. Warneck P, Wurzinger C (1988) J Phys Chem 92:6278
353. Ammar R, Monge ME, George C, D'Anna B (2010) Chemphyschem 11:3956. doi:10.1002/cphc.201000540
354. Zepp RG, Erickson DJ III, Paul ND, Sulzberger B (2007) Photochem Photobiol Sci 6:286
355. Niemi R, Martikainen PJ, Silvola J, Wulff A, Turtola S, Holopainen T (2002) Glob Chang Biol 8:361. doi:10.1046/j.1354-1013.2002.00478.x
356. Rinnan R, Impio M, Silvola J, Holopainen T, Martikainen PJ (2003) Oecologia 137:475. doi:10.1007/s00442-003-1366-5
357. Derendorp L, Holzinger R, Röckmann T (2011) Environ Chem 8:602. doi:http://dx.doi.org/10.1071/EN11024
358. Gallet C, Keller C (1999) Soil Biol Biochem 31:1151
359. Del Vecchio R, Blough NV (2004) Environ Sci Technol 38:3885
360. McNally AM, Moody EC, McNeill K (2005) Photochem Photobiol Sci 4:268
361. Brandt LA, Bohnet C, King JY (2009) J Geophys Res 114:G02004
362. Schade GW, Hofmann MR, Crutzen PJ (1999) Tellus B 51:889
363. Tarr MA, Miller WL, Zepp RG (1995) J Geophys Res 100:11403
364. Warneke C, Karl T, Judmaier H, Hansel A, Jordan A, Lindinger W, Crutzen PJ (1999) Global Biogeochem Cycles 13:9
365. Lalonde JD, Amyot M, Orvoine J, Morel FMM, Auclair JC, Ariya PA (2004) Environ Sci Technol 38:508. doi:10.1021/es034394g
366. Siciliano SD, O'Driscoll NJ, Tordon R, Hill J, Beauchamp S, Lean DRS (2005) Environ Sci Technol 39:1071. doi:10.1021/es048707z
367. McNeill VF, Grannas AM, Abbatt JPD, Ammann M, Ariya P, Bartels-Rausch T, Dominé F, Donaldson DJ, Guzman MI, Heger D, Kahan TF, Klán P, Masclin S, Toubin C, Voisin D (2012) Atmos. Chem. Phys. 12:9653